Two-photon-absorption measurements in the presence of single-photon losses

Shahram Panahiyan,[1,2] Carlos Sánchez Muñoz,[3] Maria V. Chekhova,[4,5] and Frank Schlawin[1,2,*]

[1]*Max Planck Institute for the Structure and Dynamics of Matter, Luruper Chaussee 149, 22761 Hamburg, Germany*
[2]*The Hamburg Centre for Ultrafast Imaging, Luruper Chaussee 149, 22761 Hamburg, Germany*
[3]*Departamento de Física Teórica de la Materia Condensada and Condensed Matter Physics Center, Universidad Autónoma de Madrid, 28049 Madrid, Spain*
[4]*Max-Planck Institute for the Science of Light, Staudtstraße 2, 91058 Erlangen, Germany*
[5]*University of Erlangen-Nuremberg, Staudtstraße 7/B2, 91058 Erlangen, Germany*

(Received 30 May 2022; revised 9 August 2022; accepted 19 September 2022; published 11 October 2022)

We discuss how two-photon absorption (TPA) of squeezed and coherent states of light can be detected in measurements of the transmitted light fields. Such measurements typically suffer from competing loss mechanisms such as experimental imperfections (i.e., imperfect photodetectors) and other linear scattering losses inside the sample itself, which can lead to incorrect assessments of the two-photon-absorption cross section. We evaluate the sensitivity with which TPA can be detected and find that at sufficiently large photon numbers TPA sensitivity of squeezed vacua or squeezed coherent states can become independent of linear losses that occur after the TPA event has taken place. In particular, this happens for measurements of the photon number or of the antisqueezed field quadrature, where large fluctuations counteract and exactly cancel the degradation caused by single-photon losses.

DOI: 10.1103/PhysRevA.106.043706

I. INTRODUCTION

Nonclassical quantum states of light are gaining prominence as resources for quantum-enhanced applications in imaging and spectroscopy. Of particular interest in this endeavor are nonlinear light-matter interactions, where the most stunning effects are predicted. Two-photon absorption of entangled photons or squeezed light holds great promise for imaging and spectroscopic applications, since, at low photon fluxes, the absorption probability scales linearly with the light field intensity [1–6], in contrast to the quadratic scaling of the two-photon absorption (TPA) signal induced by laser light. This remarkable effect could enable nonlinear spectroscopy and microscopy at low photon fluxes, which will be highly beneficial for photosensitive samples. To date, TPA of entangled photons or squeezed states of light was reported both in atomic gases [4,6,7] and in molecules [8–15], even though substantial controversy persists regarding the achievable enhancement of TPA signals due to entanglement in the latter case [16–19]. Entangled TPA could form the basis of new spectroscopic and microscopy applications [20–27], where quantum correlations reveal otherwise hidden features or increase the signal-to-noise ratio.

Beams of isolated entangled photon pairs, however, suffer inevitably from very low photon count rates, thus necessitating long measurement times and rendering them less appealing for practical applications. It is therefore important to also investigate quantum spectroscopy at higher photon fluxes [28]. At higher photon fluxes, entangled photon pairs start to overlap temporally to form squeezed vacuum states of light, which can contain macroscopic photon numbers [29–34], and still show interesting properties for applications. For instance, large photon-number fluctuations render them more efficient at driving higher harmonic generation in crystals than laser pulses with identical intensity [35]. These states could further provide benefits for quantum imaging [36–42] or spectroscopy [43–48], due to the reduced quadrature fluctuations of squeezed light sources. Moreover, spectral quantum correlations, which lie at the heart of quantum advantage in entangled two-photon absorption, also remain prominent in such higher-intensity states [49] and could be exploited for sensing. It is in this regime that recent experimental demonstrations of stimulated Raman imaging with squeezed light provided conclusive evidence that quantum properties of light can improve the performance of nonlinear imaging and spectroscopic applications beyond the limits of classical laser pulses [39,40,50–52]. Quantum enhancement of the signal-to-noise ratio can reduce photodamage, which constitutes a major drawback of nonlinear methods in the investigation of photosensitive biological samples, and open novel perspectives in quantum-enabled imaging technologies.

Nonlinear spectroscopy with high-flux squeezed states of light has also been discussed extensively in the theoretical literature. The application to nonlinear spectroscopy was first investigated theoretically in [53], where the distinct scaling

*frank.schlawin@mpsd.mpg.de

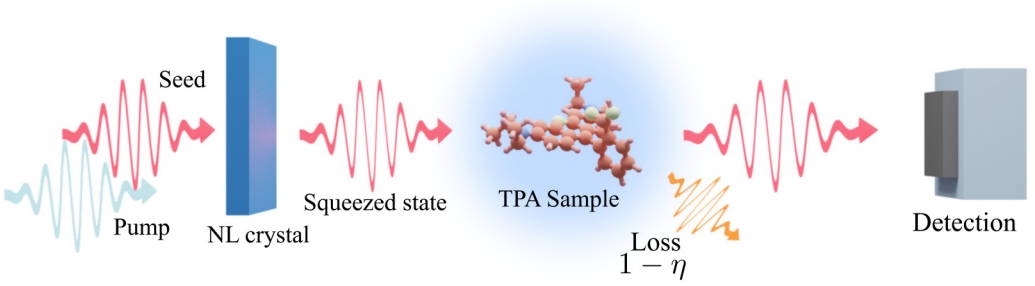

FIG. 1. Two-photon absorption in a sample is detected by measuring the transmission of a coherent or squeezed beam. A pump pulse (blue) with frequency $2\omega_0$ drives down-conversion into photons at ω_0 in a nonlinear crystal creating a squeezed state or a squeezed coherent state in case the down-conversion process is seeded (red). The output field is focused on the TPA sample and the transmitted light is detected. Single-photon losses with a loss rate $1-\eta$ can degrade the measurement outcome.

behavior of different matter pathways contributing to the signal was analyzed. The spectroscopic information contained in squeezed light emission was considered both experimentally and theoretically in [54,55]. More recent work by Michael *et al.* analyzed squeezing-enhanced detection of coherent Raman scattering in a nonlinear interferometer [56,57], demonstrating how interferometric measurements could be exploited in nonlinear spectroscopy. Finally, a recent analysis by some of the authors showed that squeezing can enhance the precision with which two-photon-absorption losses could be measured [58], based on calculations of classical and quantum Fisher information. In particular, the maximally achievable precision for determining TPA losses with quadrature measurements was shown to improve quartically with the mean photon photon number proportional to n^4. Such a scaling can only be achieved using squeezed states, while coherent (classical) states only enable a cubic scaling proportional to n^3. In other observables such as the photon number or the antisqueezed quadrature, squeezed states only realize a quadratic scaling, whereas coherent states again have a cubic dependence on the incident photon number. These results were obtained, however, in an idealized situation where no competing loss sources impede the precise measurement of the TPA. As these will be unavoidable in any experiment, however, the role of these single-photon losses remains an important open question.

In this paper, we will address it and investigate in detail the influence of single-photon losses on the measurement of the TPA absorbance of a sample. We will show that the quartic scaling mentioned above is quickly degraded even by very weak single-photon losses. In stark contrast, the sensitivity of observables that scale quadratically with the photon number becomes *independent* of these losses. Measurements with coherent states are always affected by the single-photon losses. Combining these findings, we find that amplitude-squeezed states can eliminate the degradation of the sensitivity due to the single-photon losses in measurements. As a consequence, for instance, photon-number measurements with sufficiently strongly amplitude-squeezed states can combine the superior cubic scaling of the measurement sensitivity with a robustness against degradation by noise. This insight allows us to derive an optimal degree of squeezing. It depends on the noise level, i.e., on the single-photon-loss probability due to undesirable error sources, as well as on the mean photon number of the incident photonic state.

The paper is structured as follows. In Sec. II we introduce the model of TPA losses, which we describe with a Markov master equation. We describe how losses are modeled and how signals are calculated. In Sec. III we apply this formalism to TPA measurements in transmission. We calculate the classical Fisher information (FI) in the presence of losses and investigate how the information gets eroded. In Sec. IV we summarize our findings.

II. MEASURING TWO-PHOTON ABSORPTION

A. Setup and master equation

We consider TPA measurements in a transmission geometry, as sketched in Fig. 1. An input coherent seed at frequency ω_0 is squeezed in an optical parametric amplifier (OPA), implemented by means of a nonlinear crystal pumped at frequency $2\omega_0$, and then used as a probe for a TPA measurement. We focus on a narrow-bandwidth regime, where a single mode of light is sufficient to describe the light field. The measurement is modeled in two parts. First, the light traverses a two-photon absorbing medium, where the TPA information is encoded in the quantum state. The transmitted state then undergoes single-photon losses, which could stem from scattering losses in the optical system or imperfect photon detection. Finally, an observable is measured in the detection stage (sketched here as a photon counter). In Appendix C we discuss what happens in case there are single-photon losses also inside the medium and demonstrate how this situation can be incorporated into the formalism presented in the main text.

To describe the transmission of the quantum state of light through the two-photon absorbing medium, we eliminate the material using the normal methods of open quantum systems to obtain a Markovian Lindblad equation for the density matrix of the light field. In the rotating frame with respect to the field Hamiltonian it reads (see Appendix A for more details) [59–65]

$$\frac{d}{dt}\rho = \gamma_{\mathrm{TPA}}\mathcal{L}_{\mathrm{TPA}}\rho = \frac{\gamma_{\mathrm{TPA}}}{4}(2a^2\rho a^{\dagger 2} - a^{\dagger 2}a^2\rho - \rho a^{\dagger 2}a^2). \tag{1}$$

Here a ($a^\dagger$) denotes the photon annihilation (creation) operator of the field mode. Note that, in writing Eq. (1), we write down the Lindblad operator given by a correlated loss operator $L = a^2/\sqrt{2}$, in order to simplify expressions in our

subsequent derivations. We also note that Eq. (1) assumes that no single-photon losses occur inside the TPA medium, which in turn means that no dipole-active states must exist near the photon frequency ω_0. In the remainder of this paper we will be interested in the measurement of the absorbance $\varepsilon \equiv \gamma_{\mathrm{TPA}} t$, where t is the propagation time of the light through the TPA medium.

We further model the single-photon losses as unbalanced beam-splitter transformations, where a photon is transmitted with probability η and scattered into an auxiliary mode with probability $1-\eta$. Hence, the latter denotes the probability for the photon to be lost. This level of modeling is standard in optical interferometry [66–68], as it reproduces the same input-output relations as the solution of the Heisenberg equation of motion of the photon annihilation operator undergoing single-photon losses described by a suitable master equation (see Appendix B for details) [69–71].

B. Measurement sensitivity and Cramér-Rao bounds

The sensitivity of the measurement of the absorbance ε via the expectation value of a general operator O, $\Delta\varepsilon_O$, is defined as the square root of the variance $\Delta\varepsilon_O^2$. It can be obtained from error propagation [72],

$$\Delta\varepsilon_O^2 = \frac{\mathrm{Var}(O)}{\left|\frac{\partial\langle O\rangle}{\partial\varepsilon}\right|^2}, \tag{2}$$

where the expectation value is evaluated at fixed ε. In our derivation below, we will evaluate the changes at $\varepsilon = 0$, i.e., we assume that we can approximate the transmitted density matrix as $\rho \simeq \rho_0 + \varepsilon \times (\partial\rho_0/\partial\varepsilon)$. This seems justified for most applications, as typical two-photon-absorption cross sections in molecules are very small. It is this small-ε limit that will be the focus of our attention. The generalization to finite ε is conceptually straightforward, but does not allow analytical results and thus prevents us from developing an intuitive understanding of the underlying physics.

In general, the sensitivity (2) is bounded by the classical FI $\mathcal{F}_{\mathrm{cl}}(O,\rho)$ associated with the measurement of O, which in turn is bounded by the quantum Fisher information $\mathcal{F}_Q(\rho)$, which is further maximized over any positive-operator-valued measurement [72–74],

$$\Delta\varepsilon_O^2 \geqslant \frac{1}{\mathcal{F}_{\mathrm{cl}}(O,\rho)} \geqslant \frac{1}{\mathcal{F}_Q(\rho)}. \tag{3}$$

These inequalities are known as the classical and quantum Cramér-Rao bounds, respectively. As shown in [58], the quantum FI diverges in the limit of very small absorbances $\varepsilon \to 0$ and consequently does not provide a useful tool to assess the achievable sensitivity. Instead, we will focus on the classical Fisher information in the following.

The FI of a measurement such as the detection of photon numbers is a function of the probability distribution pertaining to this measurement. Here the photon-number distribution is given by the set of probabilities $\{P_n\}$ for the detection of n photons. The information to be gained from the change of this distribution under TPA losses is quantified by the FI [73,74]

$$\mathcal{F}_C(\rho_\varepsilon,\hat{n}) = \sum_n P_n(\varepsilon)\left(\frac{\partial}{\partial\varepsilon}\ln P_n(\varepsilon)\right)^2 = \sum_n \frac{1}{P_n(\varepsilon)}\left(\frac{\partial P_n(\varepsilon)}{\partial\varepsilon}\right)^2. \tag{4}$$

It is likewise defined for operators with a continuous spectrum, which give rise to a probability distribution function. For instance, given the probability distribution $P(q)$ of possible measurement outcomes for measurements of the field quadrature $\hat{q}$, we calculate the corresponding FI

$$\mathcal{F}_C(\rho_\varepsilon,q) = \int dq \frac{1}{P(q)}\left(\frac{dP(q)}{d\varepsilon}\right)^2. \tag{5}$$

C. Measurement sensitivity for two-photon losses

We now discuss how we evaluate measurement observables and the measurement sensitivities. In the setup presented in Fig. 1, the expectation value of the operator O is formally given by

$$\langle O\rangle = \mathrm{tr}\{O e^{\mathcal{L}_{\mathrm{loss}}} e^{\mathcal{L}_{\mathrm{TPA}}\varepsilon} e^{\mathcal{L}_{\mathrm{OPA}}}\rho_0\}, \tag{6}$$

where ρ_0 is the initial state of light. In addition, $\mathcal{L}_{\mathrm{OPA}}$ is a superoperator, which describes a squeezing operation, i.e., it acts on a density matrix σ as

$$e^{\mathcal{L}_{\mathrm{OPA}}}\sigma \equiv U_{\mathrm{OPA}}\sigma U_{\mathrm{OPA}}^\dagger. \tag{7}$$

Here we define the squeezing transformation [69]

$$U_{\mathrm{OPA}} = \exp\left(\frac{\zeta}{2}a^{\dagger 2} - \frac{\zeta^*}{2}a^2\right), \tag{8}$$

with $\zeta = re^{i\phi_r}$. The second superoperator in Eq. (6), $\exp(\mathcal{L}_{\mathrm{TPA}}\varepsilon)$, describes the evolution according to the two-photon-loss Lindbladian (1). Finally, we account for single-photon losses. As described earlier, we can treat these losses via a beam-splitter transformation in which the scattering into an auxiliary photon mode with photon annihilation operator c is described by a superoperator [66–68,75,76]

$$e^{\mathcal{L}_{\mathrm{loss}}}\sigma = U_{\mathrm{loss}}\sigma U_{\mathrm{loss}}^\dagger, \tag{9}$$

where

$$U_{\mathrm{loss}} = \exp\left(\frac{\tau(ac^\dagger + ca^\dagger)}{2}\right), \tag{10}$$

with $\tau = \arccos(\sqrt{\eta})$. Here η denotes the transmission probability for a photon and $1-\eta$ quantifies the losses which are incurred by this process.

We can now calculate Eq. (2). Since only the TPA evolution depends on ε, we find straightforwardly the change of the expectation value with ε,

$$\left.\frac{\partial\langle O\rangle}{\partial\varepsilon}\right|_{\varepsilon=0} = \left.\mathrm{tr}\left\{O e^{\mathcal{L}_{\mathrm{loss}}}\frac{\partial}{\partial\varepsilon}e^{\mathcal{L}_{\mathrm{TPA}}\varepsilon}e^{\mathcal{L}_{\mathrm{OPA}}}\rho_0\right\}\right|_{\varepsilon=0} = \mathrm{tr}\{O e^{\mathcal{L}_{\mathrm{loss}}}\mathcal{L}_{\mathrm{TPA}}e^{\mathcal{L}_{\mathrm{OPA}}}\rho_0\}. \tag{11}$$

Using Eq. (7), we can rewrite Eq. (11) as an expectation value with respect to the initial state ρ_0. Defining the primed

operators $O' \equiv U_{\rm TPA}^\dagger O U_{\rm TPA}$, we obtain

$$O_f = \mathcal{L}'_{\rm TPA}[U_{\rm loss}^\dagger O' U_{\rm loss}] \tag{12}$$

and

$$\left.\frac{\partial\langle O\rangle}{\partial\varepsilon}\right|_{\varepsilon=0} = \mathrm{tr}\{O_f\rho_0\}. \tag{13}$$

Here $\mathcal{L}'_{\rm TPA}$ denotes the adjoint superoperator to Eq. (1), which acts on a operator X as

$$\mathcal{L}'_{\rm TPA}X = \tfrac{1}{4}(2a'^{\dagger 2}Xa'^2 - a'^{\dagger 2}a'^2X - Xa'^{\dagger 2}a'^2), \tag{14}$$

where we define the transformed operators $a' = U_{\rm OPA}^\dagger a U_{\rm OPA}$ and $a'^\dagger = U_{\rm OPA}^\dagger a^\dagger U_{\rm OPA}$.

Equation (13) can be translated into successive transformations of the photon operators in the Heisenberg picture.

(i) Perform squeezing operation. Using Eq. (7), we find

$$a \to a' = U_{\rm OPA}^\dagger a U_{\rm OPA} = \cosh(r)a + \sinh(r)e^{i\phi_r}a^\dagger. \tag{15}$$

Unless specified otherwise, we will set $\phi_r = 0$ in the following without loss of generality.

(ii) Apply the adjoint Lindbladian (14) to a',

$$a' \to a'' = a' + \varepsilon\mathcal{L}'_{\rm TPA}[a'] = a' - \frac{\varepsilon}{2}a'^\dagger a'^2. \tag{16}$$

(iii) Perform the beam-splitter transformation according to Eq. (10) to account for single-photon losses,

$$a'' \to a''' = \sqrt{\eta}a'' + \sqrt{1-\eta}c. \tag{17}$$

Finally, the expectation value is taken with respect to the initial state of the light field, which in the following we will assume to be either in the vacuum or in a coherent state with amplitude $\alpha = |\alpha|e^{i\phi}$ and we collect terms which are linear in ε to get the derivative.

D. Calculation of the Fisher information

In contrast to calculating expectation values, the evaluation of the classical FI requires us to determine the full probability distribution $\{P_n\}$ of measuring n photons or the continuous distribution functions $P(q)$ and $P(p)$ for the measurement of field quadratures, respectively. As described in [58], this is best done in the Schrödinger picture in a squeezed basis defined by the orthonormal basis $|\tilde{n}\rangle = U_{\rm OPA}|n\rangle$. In this basis, the squeezed vacuum state becomes the vacuum and a squeezed coherent state simply becomes a coherent state.[1] The time evolution is then given by Eq. (1), where the photon annihilation operators have to be transformed into the squeezed basis,

$$\tilde{a} = U_{\rm OPA}^\dagger a U_{\rm TPA}. \tag{18}$$

The change of the density matrix is then given by the action of the transformed Lindbladian on the ground state of the squeezed basis, i.e., $\partial\tilde{\rho}/\partial\varepsilon = \tilde{\mathcal{L}}_{\rm TPA}|\tilde{0}\rangle\langle\tilde{0}|$.

[1]We can also transform to a squeezed-displaced basis defined by $|\tilde{\tilde{n}}\rangle = U_{\rm OPA}D(\alpha)|n\rangle$, where the squeezed coherent state again becomes the vacuum.

III. RESULTS

A. Photon-number measurements

1. Squeezed vacuum

We calculate the mean photon number, i.e., the expectation value of the operator $O = a^\dagger a$, and obtain

$$\begin{aligned}\langle\hat{n}\rangle_{\rm SV} &= \eta\sinh^2(r) - \frac{\varepsilon\eta}{2}[3\cosh(2r) - 1]\sinh^2(r)\\ &= \eta n_r[1 - \varepsilon(1+3n_r)],\end{aligned} \tag{19}$$

where we use $n_r = \sinh^2(r)$ and the subscript SV indicates the squeezed vacuum. The first term is the transmission of the empty setup (without the TPA sample) and the second term, which is proportional to ε, is calculated using Eq. (13). As expected, in the imperfect detection case the TPA and linear scattering losses cannot be separated. The measurement of the change of transmission can accurately and straightforwardly measure TPA cross sections in the presence of linear losses in the sample only if one can drive the absorption process in the quadratic regime $n_r \gg 1$.

Calculating further the variation of the photon number and using Eq. (2), we obtain the sensitivity

$$\begin{aligned}\Delta\varepsilon_{\hat{n}}^{2({\rm SV})} &= \frac{1+\eta\cosh(2r)}{\eta\sinh^2(r)[1-3\cosh(2r)]^2/4}\\ &= \frac{1}{\eta n_r}\frac{1+\eta(2n_r+1)}{(1+3n_r)^2}.\end{aligned} \tag{20}$$

At large photon numbers, i.e., $n_r \gg 1$, this result simplifies to

$$\Delta\varepsilon_{\hat{n}}^{2({\rm SV})} \to \frac{2}{(3n_r)^2}, \tag{21}$$

which remarkably is independent of the linear losses described by η. This behavior is shown in Fig. 2(a), where the inverse of the sensitivity (20) is plotted as dashed lines for almost ideal setups (i.e., with transmission probability $\eta = 0.9$), intermediate case ($\eta = 0.5$), and extremely lossy setups ($\eta = 0.1$). In any case, the sensitivity converges to the limit (21) at large squeezing. The necessary photon number, for which this crossover takes place, will depend on the probability of single-photon losses, i.e., it takes place when $2\eta n_r \gg 1$ in the numerator of Eq. (20). Finally, we remark again that if we additionally take single-photon losses into account, which happen ahead of the TPA process, i.e., if the sample does not interact with a pure squeezed quantum state of light, then these losses indeed impact the sensitivity.

Fisher information. Next we focus on limits on achievable sensitivity via Fisher information according to the Cramér-Rao bound (3). We already calculated the FI (4) in [58] in the absence of single-photon losses. Here we analyze how the FI is affected by this error source.

The probability of detecting n photons after they undergo single-photon losses is given by [77]

$$P_n(\varepsilon) = \sum_{m>n}\binom{m}{n}\eta^n(1-\eta)^{m-n}P_m^{(0)}(\varepsilon), \tag{22}$$

where $P_m^{(0)}$ denotes the probability to find m photons in the light field before the single-photon losses occur. For a squeezed vacuum state with mean photon number $\bar{n}$, this

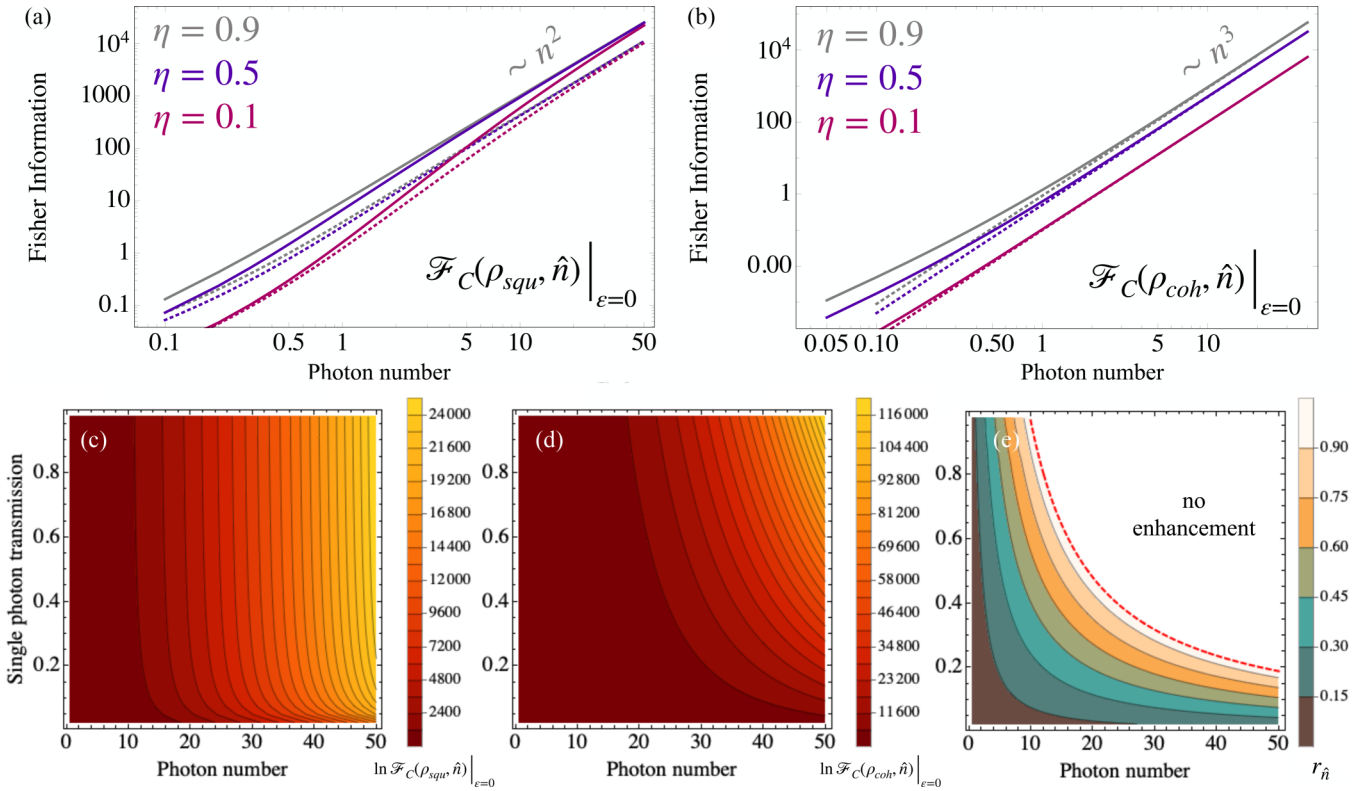

FIG. 2. (a) Fisher information (4) of photon-number measurements plotted vs the mean photon number of squeezed vacuum input states in the presence of single-photon losses with $\eta = 0.9$ (gray), 0.5 (blue), and 0.1 (red). The dashed lines correspond to the information attainable from the analysis of the mean photon number alone, i.e., the inverse of Eq. (20). (b) Fisher information (4) of photon-number measurements plotted vs the mean photon number of coherent input states in the presence of single-photon losses with $\eta = 0.9$ (gray), 0.5 (blue), and 0.1 (red). The dashed lines correspond to the information attainable from the analysis of the mean photon number alone according the inverse of Eq. (24). (c) Same as (a) plotted vs the photon number and the single-photon transmission probability η. (d) Same as (b) plotted vs the photon number and the single-photon transmission probability η. (e) Parameter regime, for which the ratio (25) is below one, plotted vs the single-photon transmission and the average photon number. The red dashed line indicates the crossover, where $r_{\hat{n}} = 1$.

probability is given by $P_m^{(0)} = (m!)\bar{n}^{m/2}2^{-m/2}[(m/2)!]^2(1+\bar{n})^{(m+1)/2}$ (for even m). The initial state, and hence its populations, undergoes TPA according to the master equation (1), which yields the change of the population distribution

$$\frac{\partial P_n^{(0)}(\varepsilon)}{\partial \varepsilon} = \frac{1}{2}\left[(n+2)(n+1)P_{n+2}^{(0)} - n(n-1)P_n^{(0)}\right]. \quad (23)$$

Together with Eq. (22), this allows us to evaluate the Fisher information (4) straightforwardly.

The FI is shown as solid lines in Fig. 2(a) for the same parameters as the sensitivity (2) discussed before, i.e., for single-photon-loss strength ranging between weak (photon transmission probability $\eta = 0.9$) and very strong losses ($\eta = 0.1$). As in our earlier analysis of the sensitivity attainable from mean-photon-number measurements in Fig. 2(a), we find that the FI converges to the "ideal" situation of vanishing single-photon losses at large photon numbers. The convergence takes place on the same photon-number range as for the sensitivity before. At each photon number, the FI is larger than the inverse of Eq. (20), such that additional information can be gained from higher statistical moments of the photon-number distribution. The scaling with photon numbers remains the same in both cases, proportional to $\langle\hat{n}\rangle^2$. The lack of dependence on the single-photon losses is further illustrated in Fig. 2(c), where the same FI is plotted vs both the photon number and the transmission probability η. At sufficiently large photon numbers, the dependence on losses can only be observed for very small η, i.e., very large photon-loss probabilities.

2. *Coherent states*

To compare the above result with a conventional TPA measurement with laser pulses, we now calculate the sensitivity achievable with transmission measurements of a coherent state with complex amplitude α. Using the TPA transformation of the photon operators in Eq. (16), we find $\partial\langle\hat{n}\rangle_{\rm coh}/\partial\varepsilon = -\eta|\alpha|^4$. Given the variance of the coherent state $\mathrm{Var}(\hat{n}) = \eta|\alpha|^2 = \langle\hat{n}\rangle_{\varepsilon=0}$, we find

$$\Delta\varepsilon_{\hat{n}}^{2\,(\rm coh)} = \frac{\eta|\alpha|^2}{\eta^2|\alpha|^8} = \frac{1}{\eta|\alpha|^6} = \frac{1}{\eta n_\alpha^3}, \quad (24)$$

where $n_\alpha = |\alpha|^2$. Crucially, since both the variance and the change of the photon number are linear in η, the influence of linear losses can never be removed from the sensitivity. In contrast, the photon-number variance of the squeezed state in Eq. (20) contains linear and quadratic terms in η. At large squeezing, the latter dominate and the η dependence cancels.

The inverse sensitivity for coherent state measurements is plotted in Fig. 2(b) vs the average photon number $|\alpha|^2$ for different single-photon-loss rates. In contrast to the squeezed state measurements in Fig. 2(a), the three dependences are parallel at sufficiently large photon numbers, with the single-photon losses accounting for a constant reduction of the sensitivity. Nevertheless, at large photon numbers coherent states can outperform squeezed vacuum states even in the presence of strong single-photon losses due to the superior, cubic scaling with the photon number proportional to $\langle\hat{n}\rangle^3$. Figure 2(d) further illustrates that this remains true for any single-photon-loss rate and any photon number. In contrast to the squeezed vacuum in Fig. 2(c), the equipotential lines do not tend to become vertical.

Fisher information. As in the squeezed vacuum case, we evaluate the FI (4) which quantifies the additional precision gains that the analysis of the full photon-counting distribution enables. We can analyze the calculations of the preceding section using the probability distribution of a coherent state as input, i.e., we evaluate Eq. (22) with $P_m^{(0)} = \exp(-\overline{n})\overline{n}^m/m!$. The results are shown as solid lines in Fig. 2(b). In contrast to the squeezed vacuum case in Fig. 2(a), the FI of coherent states and the inverse of Eq. (24) almost coincide for photon numbers $n \gtrsim 1$. Hence, as one would intuitively expect, the analysis of higher statistical moments of the measured photon distribution cannot enhance the achievable sensitivity for TPA measurements with strong coherent light, where the probability distribution is dominated by its mean value and shows only small fluctuations. Furthermore, just like in Eq. (24), we find that single-photon losses cannot be compensated and lower the FI linearly.

We summarize the comparison between squeezed vacuum and coherent states in Fig. 2(e), where we plot the ratio

$$r_{\hat{n}} \equiv \frac{\mathcal{F}_C(\rho_{\text{coh}}, \hat{n})}{\mathcal{F}_C(\rho_{\text{squ}}, \hat{n})} \tag{25}$$

between the FI of the two cases. Figure 2 shows the parameter regime for which squeezed light can outperform coherent states, i.e., where $r_{\hat{n}} < 1$. This is the case at small photon numbers or in the presence of heavy single-photon losses. We find that when single-photon losses are weak, i.e., $1 - \eta \simeq 0$, this is the case for $n \lesssim 10$.

3. *Squeezed coherent state*

Finally, we consider TPA detection with a squeezed coherent state, i.e., we assume that a coherent state with amplitude α is fed into the OPA as sketched in Fig. 1. This setup creates the state $S(\zeta)D(\alpha)|0\rangle$. We note that this state is different from the usual definition of a squeezed coherent state $|\alpha, \zeta\rangle = D(\alpha)S(\zeta)|0\rangle$ which is often found in the literature and where a squeezed vacuum is displaced. We can transform from one to the other using the identity

$$|\alpha, \zeta\rangle = S(\zeta)D(\alpha\cosh r + \alpha^* e^{i\phi}\sinh r)|0\rangle \tag{26}$$

and use, for instance, the photon-number distributions for $|\alpha, \zeta\rangle$ in [69]. With a general phase $\alpha = |\alpha|e^{i\phi}$, we obtain a phase-squeezed coherent state at $\phi = 0$ and an amplitude-squeezed state at $\phi = \pi/2$. The photon-number distributions of the two cases is shown in Fig. 3.

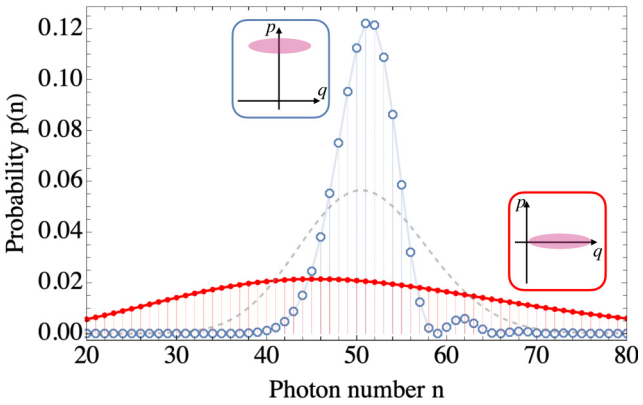

FIG. 3. Photon-number probability distributions of squeezed coherent states with fixed mean photon number $\langle\hat{n}\rangle = 50$. The open blue circles show the probability distribution of an amplitude-squeezed state, where the laser phase is set to $\phi = \pi/2$. The red points show the corresponding phase-squeezed states with $\phi = 0$. The insets sketch a phase-space picture of the respective states; the frames are colored as the respective plots. The gray dashed line finally indicates a coherent state distribution for comparison.

The average detected photon number is given by

$$\begin{aligned}\langle\hat{n}\rangle_{\text{sq-coh}} = \eta\{&n_r + |\alpha|^2[1 + 2n_r + \cos(2\phi)2\sqrt{n_r(1+n_r)}]\}\\ &+ \varepsilon\eta\{(n_r + 3n_r^2) + 2|\alpha|^2[2n_r(2 + 3n_r)\\ &+ \cos(2\phi)\sqrt{n_2(1+n_r)}(1 + 6n_r)]\\ &+ |\alpha|^4[1 + 6n_r(1 + n_r)\\ &+ 4\cos(2\phi)\sqrt{n_r(1+n_r)}(1 + 2n_r)\\ &+ 2\cos(4\phi)n_r(1 + n_r)]\}.\end{aligned} \tag{27}$$

We remind the reader that we use the abbreviation $n_r = \sinh^2(r)$. The subscript sq-coh distinguishes it from the squeezed vacuum calculation in Eq. (19). The photon-number variance at $\varepsilon = 0$ is given by

$$\begin{aligned}\text{Var}(\hat{n}) =&\eta n_r[1 + \eta(1 + 2n_r)]\\ &+ \eta|\alpha|^2\{1 + 2n_r + \cos(2\phi)\sqrt{n_r(1+n_r)}\\ &+ 2\eta[n_r(3+4n_r) + \cos(2\phi)\sqrt{n_r(1+n_r)}(1+4n_r)]\}.\end{aligned} \tag{28}$$

The phase dependence of the resulting sensitivity is plotted in Fig. 4. We fix the mean photon number that interacts with the sample; it is simply given by Eq. (27) at $\varepsilon = 0$ and $\eta = 1$ (i.e., before any losses have taken place). Overall, we find that amplitude-squeezed state states with $\phi = \pi/2$ perform better than phase-squeezed states at $\phi = 0$. As we choose a fairly large mean photon number $\langle\hat{n}\rangle_{\text{sq-coh}} = 10$ and no single-photon losses, a large coherent amplitude is beneficial due to its cubic scaling [see Eq. (24)] such that a weakly squeezed state generally performs better than a more strongly squeezed state or a squeezed vacuum state. In any case, however, we find that amplitude squeezing can provide an advantage, while phase squeezing appears to be the least effective way to increase the sensitivity.

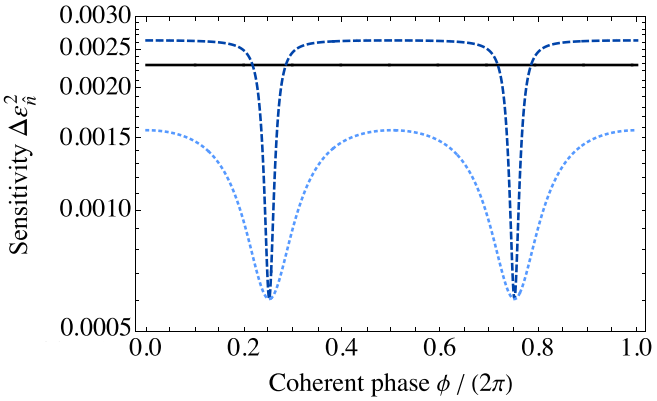

FIG. 4. Phase dependence of the sensitivity (2) for measurements with a squeezed coherent state with mean photon number $\langle\hat{n}\rangle = 10$ and squeezing parameters $r = 0.88$ (dark blue dashed line) and $r = 0.31$ (light blue dotted line). For each phase, we adjust the coherent amplitude α such that the mean photon number remains constant. The black solid line indicates the squeezed vacuum sensitivity at $\langle\hat{n}\rangle = 10$. We further set $\eta = 1$, i.e., we consider an ideal setup without any single-photon losses.

At large squeezing $n_r \gg 1$, the leading contributions give, using the definition of the sensitivity (2),

$$\Delta\varepsilon^{2(\mathrm{sc})}_{\hat{n}} \to \frac{2\eta^2|\alpha|^2\left[4n_r^2 + \cos(2\phi)4n_r^2\right]}{\left\{\eta|\alpha|^4\left[6n_r^2 + 8n_r^2\cos(2\phi) + 2n_r^2\cos(4\phi)\right]\right\}^2} = \frac{4[1+\cos(2\phi)]}{|\alpha|^6 n_r^2(16\cos^4\phi)^2}. \tag{29}$$

At $\phi = 0$, i.e., a phase-squeezed state, this simplifies to

$$\Delta\varepsilon^2_{\hat{n},p\text{-}s} \simeq \frac{1}{|\alpha|^6 e^{4r}} = \frac{1}{|\alpha|^2|\alpha e^r|^4}. \tag{30}$$

The subscript p-s is introduced to denote the phase squeezing. Hence, the squeezed coherent state still shows the cubic scaling of the coherent input (i.e., $\sim|\alpha|^6$). However, a sufficiently strong squeezing component can compensate for the detrimental influence of single-photon losses and render the sensitivity independent of the transmission probability η. For an amplitude-squeezed state with $\phi = \pi/2$, we find that both leading-order terms in the numerator and denominator vanish and the subleading contributions then yield the sensitivity

$$\Delta\varepsilon^2_{\hat{n},a\text{-}s} \simeq \frac{1}{|\alpha|^6 e^{2r}}. \tag{31}$$

Thus, at a first glance, it appears that the phase-squeezed state (30) is capable of detecting TPA losses with higher precision. However, this changes completely when we relate the scaling to the incident photon number [Eq. (27) at $\varepsilon = 0$ and $\eta = 1$], where we find $\langle\hat{n}\rangle_{p\text{-}s} \simeq |\alpha e^r|^2$ and $\langle\hat{n}\rangle_{a\text{-}s} \simeq |\alpha e^{-r}|^2$, respectively, at large α. Here we have neglected the spontaneously down-converted photons $\sim\sinh^2 r$. Plugging these back into the sensitivities (30) and (31), we find $\Delta\varepsilon^2_{\hat{n},p\text{-}s} \simeq e^{2r}\langle\hat{n}\rangle^{-3}$ and $\Delta\varepsilon^2_{\hat{n},a\text{-}s} \simeq e^{-4r}\langle\hat{n}\rangle^{-3}$. The squeezing thus deteriorates the sensing capabilities of the phase-squeezed state. The increase in the mean photon number is more than counterbalanced by the increased photon-number fluctuations (compare Fig. 3).

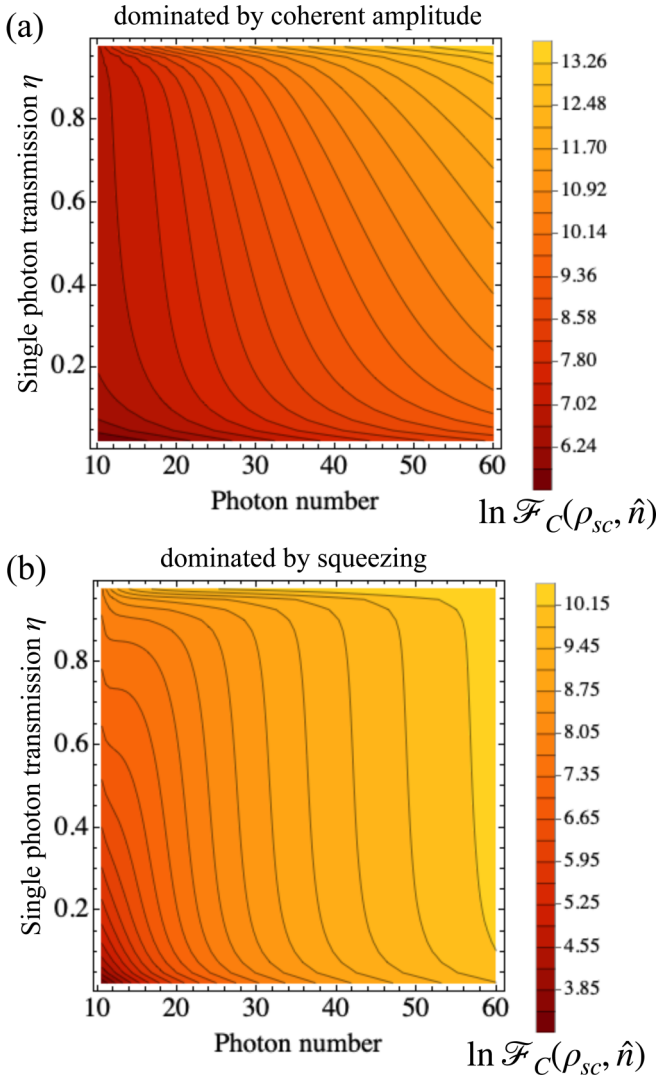

FIG. 5. (a) Logarithm of the Fisher information (4) for an amplitude-squeezed coherent state (i.e., $\phi = \pi/2$), which is dominated by its coherent amplitude, shown vs the transmission probability η and the average photon number. The squeezing parameter is fixed as $r = 1.876$ (corresponding to a photon number $\simeq$10 in a squeezed vacuum state) and the coherent amplitude is increased to produce the desired average photon number. (b) Same as (a) but for a state with fixed coherent amplitude $\alpha = \sqrt{10}$ and variable squeezing parameter.

The opposite is true for the amplitude-squeezed state: While the squeezing operation reduces the initial number of photons in the coherent state $\alpha \to \alpha e^{-r}$, the resulting state shows exponentially enhanced sensitivity at a given average photon number.

Fisher information. We finish this section by evaluating the FI (4) in the presence of single-photon losses with squeezed coherent input states. In Figs. 5(a) and 5(b) we present parameter scans of the FI vs the transmission probability η and the average photon number for two extreme cases: We keep the squeezing parameter r fixed in Fig. 5(a), producing a state with substantial squeezing but whose large-n behavior is dominated by the coherent amplitude

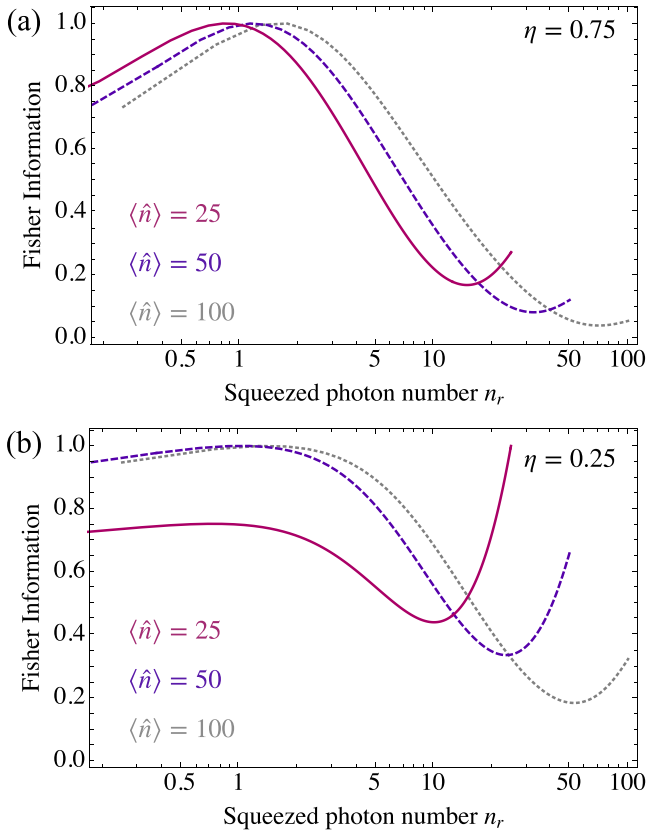

FIG. 6. (a) Fisher Information (4), normalized to its optimal value, plotted vs the squeezed photon number $n_r = \sinh^2(r)$ at fixed single-photon transmission probability $\eta = 0.75$ and average photon number $\langle\hat{n}\rangle = 25$ (red solid line), $\langle\hat{n}\rangle = 50$ (blue dashed line), and $\langle\hat{n}\rangle = 100$ (gray dotted line). We also set the coherent amplitude phase $\phi = \pi/2$, i.e., we focus on the amplitude-squeezed states that proved superior in Fig. 4. (b) Same as (a) but for $\eta = 0.25$.

α. Conversely, we fix this coherent amplitude in Fig. 5(b) and increase the squeezing parameter r. We find that the former states are much more strongly affected by single-photon losses. Nevertheless, as they show a cubic scaling at large photon numbers proportional to n^3, the absolute FI can still become substantially larger than in the corresponding squeezing-dominated case. At fixed photon number, an optimal state will therefore contain the minimal amount of squeezing, which should be chosen sufficiently large to counter single-photon losses, but not larger than this. This makes it possible to benefit from the positive properties of the squeezed vacuum state, while also benefiting from the superior photon-number scaling of the coherent state. This is illustrated in Fig. 6, where the FI of an amplitude-squeezed state is plotted vs the squeezed photon number $n_r = \sinh^2(r)$ at fixed total average photon number. This means that with increasing r, the coherent amplitude is reduced to keep $\langle\hat{n}\rangle$ fixed. Each plot then terminates at a maximal squeezing parameter when the coherent amplitude vanishes, and $\langle\hat{n}\rangle = \sinh^2(r_{\max})$. Furthermore, to compare different photon numbers, we normalize each plot to the maximal FI. In Fig. 6(a) simulations are shown for fairly weak single-photon losses $1 - \eta = 0.25$. We find that indeed the FI increases first at small r, reaches its maximum, and then drops to a minimum, before starting to increase again when the squeezed contribution becomes dominant. When the single-photon losses are increased in Fig. 6(b), this increase at strong squeezing becomes more pronounced until it crosses the local maximum at smaller squeezing parameters. This is the case for $\langle\hat{n}\rangle = 25$ in Fig. 6(b), which means that the optimal state is a squeezed vacuum and we have reached the phase-space region shown in Fig. 2(e), where squeezed states outperform coherent states.

B. Quadrature measurements

We next turn to measurements of the field position $q = (a + a^\dagger)/\sqrt{2}$ and the momentum quadrature $p = (a - a^\dagger)/\sqrt{2}i$. We remind the reader that in Eq. (15) we set the phase of squeezing $\phi_r = 0$. This means that, if squeezing is present, the quadrature $\hat{p}$ will become squeezed, while $\hat{q}$ will be antisqueezed.

1. Squeezed vacuum

For a squeezed vacuum state, the expectation value of either quadrature vanishes, i.e., $\langle\hat{q}\rangle = \langle\hat{p}\rangle = 0$. Consequently, the sensitivity according to Eq. (2) diverges, and in order to assess the metrological power of quadrature measurements in the presence of noise, we need to turn to the FI.

Fisher information. In the presence of losses into an auxiliary mode c, we can use the transformation (17) to write the detected quadrature as

$$\hat{q}_{\text{detect}} = \sqrt{\eta}\hat{q} + \sqrt{1-\eta}\hat{q}_c, \tag{32}$$

where we added the vacuum quadrature $\hat{q}_c = (c + c^\dagger)/\sqrt{2}$, which gives rise to a probability distribution $P_c(q)$ induced by these losses. As the auxiliary mode is in the vacuum, we have simply $P_c(q) = (2/\pi)^{1/2}\exp(-2q^2)$. Defining the random variables $A \equiv \sqrt{\eta}\hat{q}$ and $B \equiv \sqrt{1-\eta}\hat{q}_c$, we find the distribution of $\hat{q}_{\text{detect}}$ as the sum of two independent random variables such that the resulting probability distribution is given by the sum of those of the two random variables

$$P(q) = \int_{-\infty}^{\infty} P_0\left(\frac{q}{\sqrt{\eta}} - \sqrt{\frac{1-\eta}{\eta}}q'\right)P_c(q')\frac{dq'}{\sqrt{\eta}}, \tag{33}$$

where P_0 denotes the probability distribution in the absence of losses. Thus, single-photon losses lead to a rescaling of the detected quadrature distribution, i.e., $q \to \sqrt{\eta}q$, as well as a convolution with the Gaussian distribution of the vacuum mode c.

In [58] we calculated the FI for quadrature measurements of squeezed vacua in the absence of losses. In particular, we found a quartic scaling behavior at large photon numbers for measurements of the squeezed quadrature,

$$\mathcal{F}_C^0(\rho_{\text{squ}}, \hat{p}) \sim 32n^4, \tag{34}$$

and a quadratic scaling of the antisqueezed quadrature,

$$\mathcal{F}_C^0(\rho_{\text{squ}}, \hat{q}) \sim \frac{21n^2}{2}. \tag{35}$$

Note that in Eqs. (34) and (35) we only show the dominant scaling contribution at large photon number n. We investigate

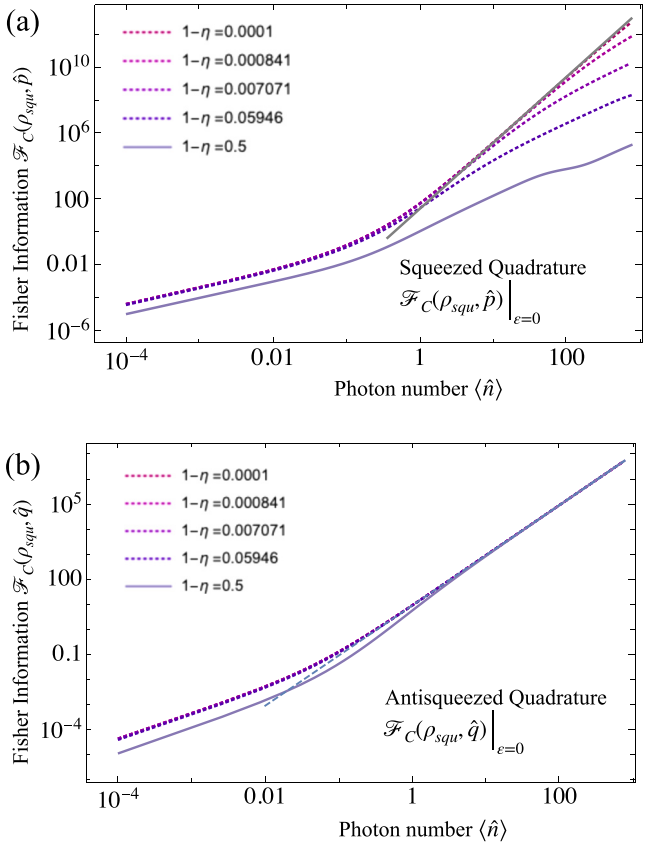

FIG. 7. (a) Scaling of the Fisher information of squeezed quadrature measurements (33) for a squeezed vacuum input state plotted vs the average photon number. The gray solid line indicates the ideal scaling behavior (34). (b) Same as (a) but for measurements of the antisqueezed quadrature. The gray solid line indicates the corresponding scaling (35) of the FI at large photon numbers.

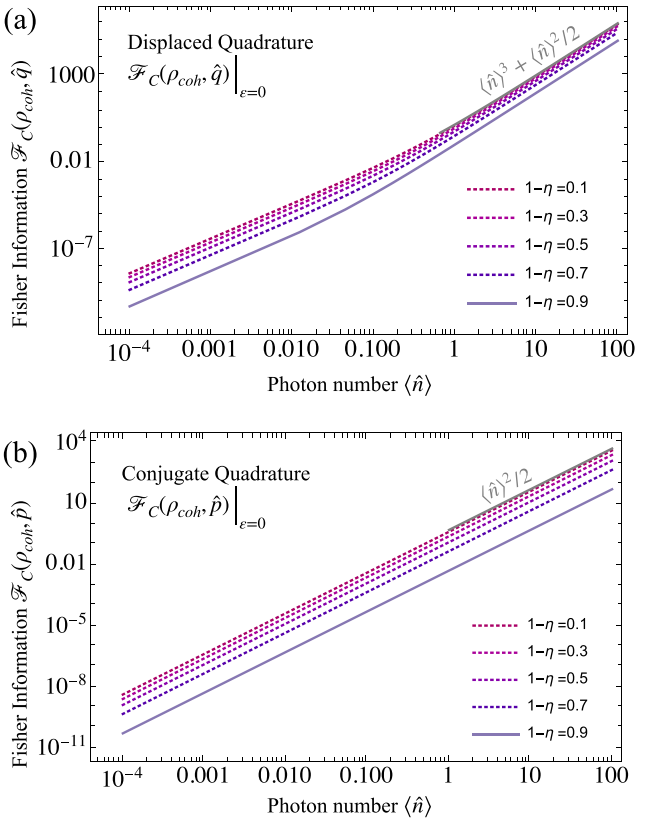

FIG. 8. (a) Scaling of the Fisher information of displaced quadrature measurements (33) for a coherent input state plotted vs the average photon number. The gray solid line indicates the ideal scaling behavior (38). (b) Same as (a) but for measurements of the momentum quadrature. The gray solid line indicates the corresponding scaling (39) of the FI at large photon numbers.

the degradation of these scaling behaviors by single-photon losses in Fig. 7. The FI of squeezed quadrature measurements is plotted in Fig. 7(a). Evidently, even for tiny losses $1-\eta < 10^{-2}$ the quartic scaling (34) is eroded substantially, and for $1-\eta = 0.5$ the scaling is lost entirely. This is quite different for the antisqueezed quadrature in Fig. 7(b). For any loss rate $1-\eta$, the FI eventually approaches the optimal scaling (35). As in our discussion of Fig. 9 below, we find that measurements of the antisqueezed quadrature are not affected by single-photon losses, provided the initial squeezing can overcome the loss rate.

2. Coherent state

For coherent input states, we obtain straightforwardly $\langle q\rangle^{(\mathrm{coh})} = \sqrt{2\eta}|\alpha|\cos(\phi)(1-\frac{\varepsilon}{2}|\alpha|^2)$ and $\langle p\rangle^{(\mathrm{coh})} = \sqrt{2\eta}|\alpha|\sin(\phi)(1-\frac{\varepsilon}{2}|\alpha|^2)$, as well as $\mathrm{Var}(p)=\mathrm{Var}(q)=\frac{1}{2}$. Hence, the sensitivity yields

$$\Delta\varepsilon_{\hat{q}}^{2\,(\mathrm{coh})} = \frac{1}{\eta|\alpha|^6\cos^2(\phi)}, \tag{36}$$

$$\Delta\varepsilon_{\hat{p}}^{2\,(\mathrm{coh})} = \frac{1}{\eta|\alpha|^6\sin^2(\phi)}. \tag{37}$$

In either case, quadrature measurements can only achieve the same sensitivity as photon-number detection [Eq. (24)], but never exceed it. They are further limited by single-photon losses η which cannot be removed or circumvented.

Fisher information. We can calculate the FI of coherent state measurements using the same approach as in the squeezed vacuum case. In [58] we derived the classical FI in an ideal setup. For a coherent state displaced along the $\hat{q}$ quadrature, we found

$$\mathcal{F}_C^0(\rho_{\mathrm{coh}},\hat{q}) = n^3 + \frac{n^2}{2} \tag{38}$$

and

$$\mathcal{F}_C^0(\rho_{\mathrm{coh}},\hat{p}) = \frac{n^2}{2}. \tag{39}$$

The simulations in the presence of losses are shown in Fig. 8. As in the photon-number measurements, we find that the FI of both measurements is affected by single-photon losses. We never observe a convergence to the ideal setup, as we did in the antisqueezed quadrature measurements before. However, it should also be noted that the degradation is not as dramatic as the reduction in Fig. 7(a) of the FI of squeezed quadrature measurements of a squeezed vacuum.

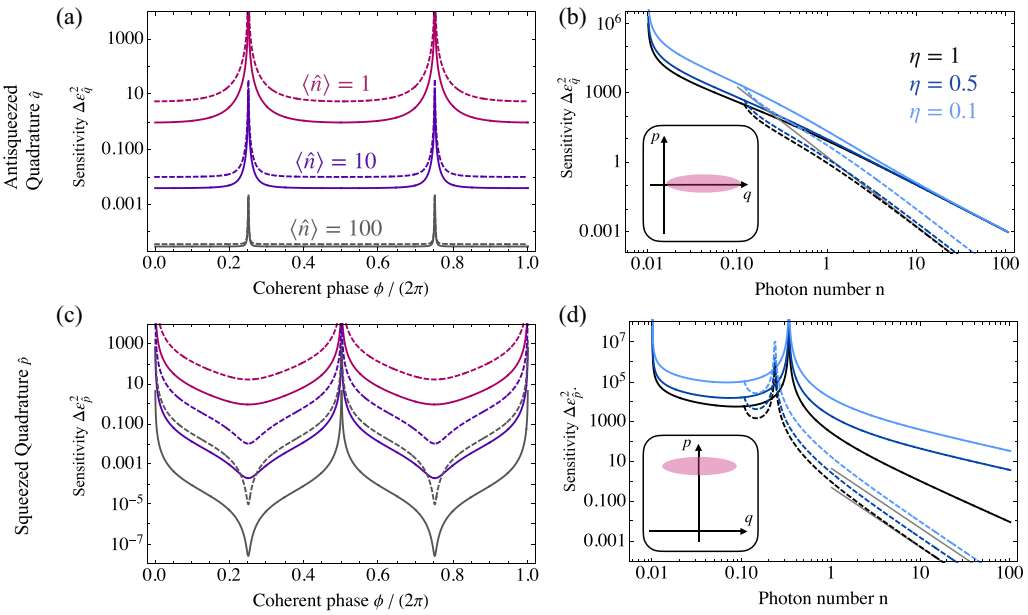

FIG. 9. (a) Sensitivity $\Delta\varepsilon^2_{\hat{q}}$ for antisqueezed q-quadrature measurements plotted for different mean photon numbers vs the coherent state phase ϕ. The solid lines show an ideal measurement with $\eta = 1$ and the dashed lines a very noisy measurement with $\eta = 0.1$. (b) Sensitivity $\Delta\varepsilon^2_{\hat{q}}$ plotted vs the mean photon number for different single-photon transmission probabilities η. The solid lines correspond to squeezed coherent states, where the coherent amplitude is fixed at $\alpha = 0.1$ and the squeezing parameter r is increased to generate larger photon numbers. The laser phase is fixed at $\phi = 0$. The light gray line indicates the limiting behavior $e^{2r}/\langle\hat{n}\rangle^3$. The inset shows a sketch of the quadrature distribution of the incident phase-squeezed state. (c) Same as (a) but for squeezed quadrature measurements $\Delta\varepsilon^2_{\hat{p}}$. The dashed lines, in contrast, correspond to states where we set $r = \sinh^{-1}(\sqrt{0.1})$ and increase the coherent amplitude α. (d) Same as (b) but for $\Delta\varepsilon^2_{\hat{p}}$. The light gray lines indicate the limiting behavior $(1-\eta)\eta^{-1}e^{-2r}\langle\hat{n}\rangle^{-3}$ for $\eta = 0.1$ and 1. The laser phase is fixed at $\phi = \pi/2$. The inset again shows the corresponding phase-space distribution.

3. *Squeezed coherent state*

We obtain for a squeezed coherent input state the expectation value

$$\langle q\rangle = \sqrt{2\eta}\alpha\cos(\phi)e^{r} - \frac{\varepsilon}{2}\sqrt{\frac{\eta}{2}}\alpha\cos(\phi)e^{r}[4n_r + \sqrt{n_r(1+n_r)} + |\alpha|^2 f_r(\phi)], \tag{40}$$

where we define the factor $f_r(\phi) = 1 + 2n_r + \cos(2\phi)2\sqrt{n_r(1+n_r)} = 2\cosh(2r) + 2\cos(2\phi)\sinh(2r)$, which determines the seed amplification, and for optimal amplification at $\phi = 0$, i.e., for a phase-squeezed state, it evaluates simply to $f_r(0) = 2\exp(2r)$ and for an amplitude-squeezed state $\phi = \pi/2$ it evaluates to $f_r(\pi/2) = 2\exp(-2r)$. The variance at $\varepsilon = 0$ yields

$$\mathrm{Var}(\hat{q}) = \tfrac{1}{2}e^{r}[\sqrt{1+n_r} + \sqrt{n_r}(2\eta - 1)]. \tag{41}$$

For measurements of the squeezed quadrature, we likewise obtain

$$\langle p\rangle = \sqrt{2\eta}\alpha\sin(\phi)e^{-r} - \frac{\varepsilon}{2}\sqrt{\frac{\eta}{2}}\alpha\sin(\phi)e^{-r}[4n_r - \sqrt{n_r(1+n_r)} + |\alpha|^2 f_r(\phi)] \tag{42}$$

and

$$\mathrm{Var}(\hat{p}) = \tfrac{1}{2}e^{-r}[\sqrt{1+n_r} - \sqrt{n_r}(2\eta - 1)]. \tag{43}$$

These results are readily plugged into Eq. (2) to obtain the sensitivity for measurements using the expectation value. At large squeezing $n_r \simeq \exp(2r)/4 \gg 1$, the expression for the antisqueezed quadrature simplifies to

$$\Delta\varepsilon^2_{\hat{q}} = \frac{\mathrm{Var}(\hat{q})}{|\partial\langle q\rangle/\partial\varepsilon|^2} \tag{44}$$

$$\simeq \frac{8\eta\sqrt{n_r}e^{r}}{\eta|\alpha\cos(\phi)|^2 e^{2r}[5n_r + |\alpha|^2 f_r(\phi)]^2} = \frac{4}{|\alpha\cos(\phi)|^2[5n_r + |\alpha|^2 f_r(\phi)]^2}. \tag{45}$$

The sensitivity is maximized at $\phi = 0, \pi, \ldots$. As we have seen in the discussion of photon-number measurements earlier, however, one has to be careful with the assessment, as the sensitivity is not yet normalized to the incident photon flux. Yet if we plot the sensitivity vs the laser phase for fixed photon numbers in Fig. 9(a), we find that indeed $\phi = 0$, i.e., a phase-squeezed state, is the optimal coherent setting for the detection of the antisqueezed quadrature. Further, we can encounter two limiting cases. When the coherent amplitude is very small, i.e., $\alpha \ll 1$, the sensitivity approaches $\Delta\varepsilon_q \to (25|\alpha|^2 e^{4r}/16)^{-1}$. Translating this into a photon-number dependence, this means $(25|\alpha|^2 e^{4r}/16)^{-1} \simeq e^{-2r}(25\langle\hat{n}\rangle/32)^{-1}$. In contrast, when the coherent seed dominates $\alpha \gg e^{r}$, the sensitivity is given by $\Delta\varepsilon_q \to (|\alpha|^6 e^{4r})^{-1} = e^{2r}/\langle\hat{n}\rangle^3$. This reproduces the scaling behavior of photon-number measurements in Eq. (30). These distinct scaling behaviors are shown in Fig. 9(b). The solid lines depict the sensitivity (44) of

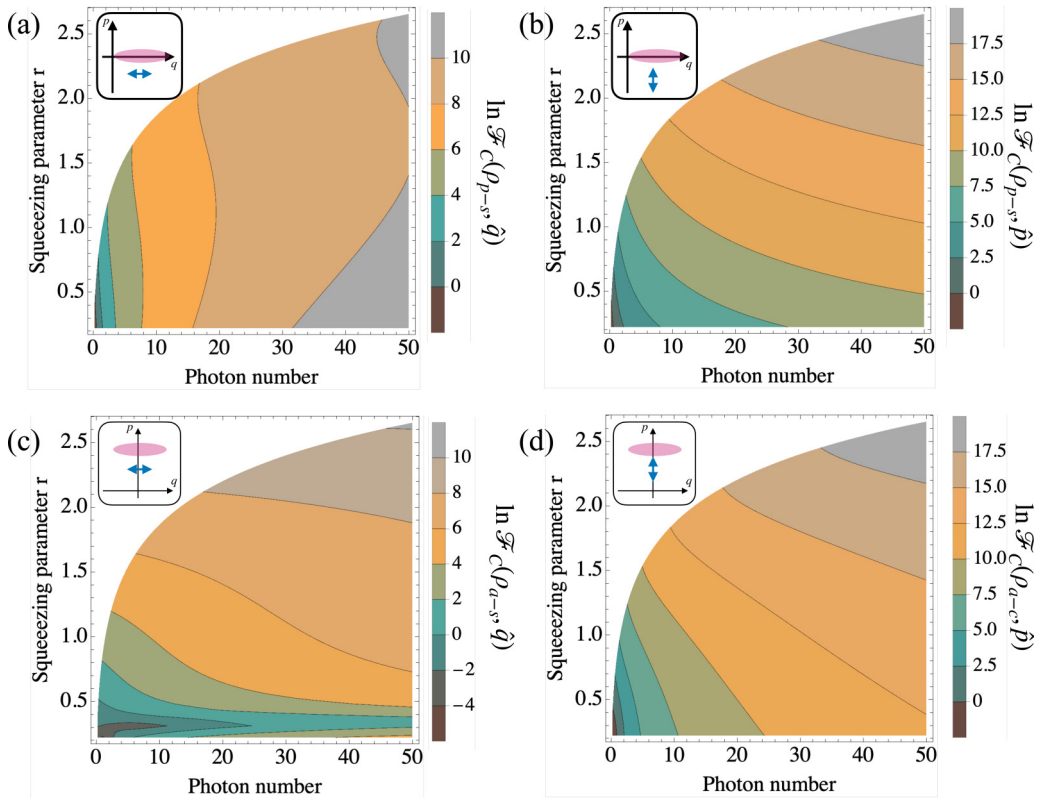

FIG. 10. (a) Logarithm of the Fisher information (5) for measurements of the antisqueezed quadrature $\hat{q}$ for phase-squeezed state $\rho_{p\text{-}s}$ shown vs the average photon number of the incident state and the squeezing parameter r. Single-photon losses are not taken into account, i.e., we set $\eta = 1$. The inset shows an illustration of the state in phase space. The blue double-arrow indicates the quadrature measurement. (b) Same as (a) but for measurements of the antisqueezed quadrature $\hat{p}$. (c) Same as (a) but for measurements with an amplitude-squeezed state $\rho_{a\text{-}s}$. (d) Same as (b) but for measurements with an amplitude-squeezed state.

states which are dominated by their squeezed contribution. Therefore, they basically reproduce the scaling behavior of squeezed vacua in Fig. 2(a). If the squeezed coherent state is instead dominated by the coherent amplitude, we rather observe an inverse cubic scaling of the sensitivity.

Running the same analysis with the sensitivity of the squeezed $\hat{p}$ quadrature, we arrive at

$$\Delta\varepsilon_{\hat{p}}^2 = \frac{\mathrm{Var}(\hat{p})}{|\partial\langle p\rangle/\partial\varepsilon|^2} \tag{46}$$

$$= \frac{8e^{-r}(1-\eta)\sqrt{n_r}}{\eta|\alpha\sin(\phi)|^2 e^{-2r}[3n_r + |\alpha|^2 f_r(\phi)]^2}$$

$$\simeq \frac{1-\eta}{\eta}\frac{4}{|\alpha\sin(\phi)|^2[3n_r + |\alpha|^2 f_r(\phi)]^2}. \tag{47}$$

Here we have approximated the numerator $\mathrm{Var}(\hat{p}) \simeq (1-\eta)n_r^{1/2}\exp(r)$, which is valid for $n_r \gg 1$. First, we note that the impact of single-photon losses, described by the transmission factor η (and loss rate $1-\eta$), cannot be eliminated from the expression. Furthermore, the sensitivity is largest when $\phi = \pi/2, 3\pi/2, \ldots$, i.e., when we prepare an amplitude-squeezed state [see Fig. 9(c)]. We again distinguish two limiting behaviours. For $\alpha \ll 1$, we find $\Delta\varepsilon_{\hat{p}}^2 \simeq (1-\eta)\eta^{-1}4(3\alpha e^{2r}/4)^2 \simeq (1-\eta)\eta^{-1}32e^{-6r}/9\langle\hat{n}\rangle$, where $\langle\hat{n}\rangle \simeq |\alpha e^{-r}|^2$. At large coherent amplitudes, we instead find $\Delta\varepsilon_{\hat{p}}^2 \simeq (1-\eta)\eta^{-1}e^{-2r}\langle\hat{n}\rangle^{-3}$.

We note that this scaling changes in an ideal measurement where $\eta = 1$. In this case, we obtain $\mathrm{Var}(\hat{p}) = e^{-2r}/2$ (rather than the noisy limit $1-\eta$ used above), and an identical calculation shows that the sensitivity approaches (for a weakly seeded squeezed state with $\alpha \ll 1$) $\Delta\varepsilon_p^{(\mathrm{ideal})} \to 32e^{-6r}/9\langle\hat{n}\rangle$. For a strongly seeded state with $\alpha \gg e^r$, we likewise obtain $\Delta\varepsilon_p^{(\mathrm{ideal})}(\phi = \pi/2) \to 2e^{-2r}/\langle\hat{n}\rangle^3$. However, the scaling remains inferior to the performance in photon-number measurements [see Eq. (31)].

Equation (46) is plotted in Fig. 9(d) for different levels of single-photon loss and for states with varying degrees of squeezing (solid lines) and varying coherent amplitudes (dashed lines). We observe a very interesting crossover between a low-photon regime, where the constant terms in the plot dominate, followed by a crossover regime where the coherent amplitude and the squeezing parameter give rise to similar photon numbers. Remarkably, in the course of this crossover the sensitivity diverges, since $\partial\langle\hat{p}\rangle/\partial\varepsilon$ changes sign when the α-dependent term becomes larger than the second term in Eq. (42). The approximate scaling behaviors are observed only at much larger mean photon numbers.

Fisher information. We finally simulate the FI of quadrature measurements with squeezed coherent states in Fig. 10. For an ideal setup without single-photon losses, we present the FI of both quadrature measurements as a function of the average incident photon number and the squeezing parameter for phase- and the amplitude-squeezed states. In our

TABLE I. Summary of analytical results for sensitivities of different states and measurement approaches.

Measurement	State	Sensitivity $\Delta\epsilon^2$	
		Limit	Formula
photon counting	squeezed vacuum	$n_r \gg 1$	$\frac{2}{9\eta^2}$
photon counting	coherent state		$\frac{1}{\eta n^3}$
photon counting	squeezed coherent $\phi = 0$ (phase squeezed)	$n_r \gg 1$	$\frac{e^{2r}}{n^3}$
photon counting	squeezed coherent $\phi = \frac{\pi}{2}$ (amplitude squeezed)	$n_r \gg 1$	$\frac{e^{-4r}}{n^3}$
antisqueezed q quadrature	coherent state		$\frac{1}{\eta n^3 \cos^2\phi}$
antisqueezed q quadrature	squeezed coherent $\phi = 0$ (phase squeezed)	$\alpha \ll 1$	$e^{-2r}\frac{32}{25n}$
antisqueezed q quadrature	squeezed coherent $\phi = 0$ (phase squeezed)	$\alpha \gg e^r$	$\frac{e^{2r}}{n^3}$
squeezed p quadrature	coherent state		$\frac{1}{\eta n^3 \sin^2\phi}$
squeezed p quadrature	squeezed coherent $\phi = \pi/2$ (amplitude squeezed)	$\alpha \ll 1$	$\frac{1-\eta}{\eta}e^{-6r}\frac{32}{9n}$
squeezed p quadrature	squeezed coherent $\phi = \pi/2$ (amplitude squeezed)	$\alpha \gg 1$	$\frac{1-\eta}{\eta}e^{-2r}\frac{1}{n^3}$

presentation, the horizontal line at $r = 0$ corresponds to the FI of coherent states. Conversely, the upper boundary, where we have maximal squeezing, corresponds to a squeezed vacuum and the coherent amplitude vanishes, i.e., $\alpha = 0$. In between these two extreme cases, the relative strength of coherent and squeezed contributions is varied continuously.

Measurements of the antisqueezed quadrature are shown in Figs. 10(a) and 10(c). In the former case [Fig. 10(a)] we find cubic growth of the FI according to Eq. (38) such that, at any fixed photon number, squeezing merely reduces the FI. In Fig. 10(c), on the other hand, it grows quadratically according to Eq. (39), such that the squeezed vacuum ultimately shows superior FI. We also note that, as in the case of the sensitivity in Eq. (46), the FI goes through a local minimum as a function of the squeezing, before growing to the squeezed vacuum case.

In Figs. 10(b) and 10(d) we show the FI pertaining to measurements of the squeezed quadrature. Here we find weaker differences between the phase-squeezed state in Fig. 10(b) and its amplitude-squeezed counterpart in Fig. 10(d). In both cases, the optimal state at large photon numbers is the squeezed vacuum due to its quartic increase according to Eq. (34).

IV. CONCLUSION

In summary, we have investigated the detection of two-photon absorption in the presence of competing single-photon losses, which could stem from scattering losses or imperfect photon detectors. Focusing on the regime of very weak TPA losses, we provided an extensive analysis of the sensitivities achievable with different observables, namely, the photon number, and the two field quadratures. A summary of the scaling behaviors we derived is provided in Table I. Note that in the quadrature measurement results, we only list phase-squeezed (amplitude-squeezed) states in measurements of the antisqueezed (squeezed) quadrature. As the expectation value of the antisqueezed (squeezed) quadrature vanishes for an amplitude-squeezed (phase-squeezed) state, the corresponding variance $\Delta\varepsilon^2$ diverges.

For photon-number measurements, our main result is that the TPA detection sensitivity measured with squeezed vacuum states can become independent of single-photon losses, provided the mean photon number of the incident state is sufficiently large. In this high-intensity regime, the change in the observable's expectation value due to single-photon losses is exactly canceled by the corresponding change of the photon-number variance. This cancellation persists also for the corresponding Fisher information, thus canceling the detrimental effect of the single-photon losses. It does not occur in measurements with coherent probe states, where the sensitivity is always reduced by unwanted losses. However, the latter sensitivity shows a superior cubic scaling with the photon number such that coherent probes will still perform better at very large photon fluxes. Moreover, we found that coherent state measurements are determined entirely by the field expectation values. The calculation of the FI shows that higher-order correlation measurements do not improve the sensitivity. This is in contrast to squeezed probes, where the FI is always roughly a factor 2 larger than the sensitivity derived from the photon-number expectation value.

In our analysis of quadrature measurements, we found that measurements of the squeezed quadrature are strongly affected by additional losses. The beneficial quartic scaling of the FI alluded to in the Introduction is quickly eroded even by very small single-photon losses. In contrast, the antisqueezed quadrature fluctuations compensate for these losses and become independent thereof. However, as in the case of photon-number measurements, this comes at the price of a suboptimal quadratic scaling with the mean photon number.

Finally, we also investigated measurements with squeezed coherent states, where we found that suitable tuning of the parameters of the light allows us to combine the positive aspects of both squeezed and coherent probes. In particular, in photon counting experiments, single-photon losses can be compensated, provided the squeezing is sufficiently large to counteract the losses. Too much squeezing, however, has a detrimental effect on the sensitivity by reducing the superior cubic scaling of coherent probes. The competition between these two effects leads us to define optimal degrees of squeezing for a given mean photon number and noise level. This behavior is true for both amplitude- and phase-squeezed states of light (see Table I). However, the latter states suffer from exponentially large photon-number fluctuations such that an amplitude-squeezed state is beneficial for TPA measurements. This is no longer true in quadrature measurements, where the squeezed quadrature is always affected by single-photon losses.

ACKNOWLEDGMENTS

S.P. and F.S. acknowledge support from the Cluster of Excellence "CUI: Advanced Imaging of Matter" of the Deutsche Forschungsgemeinschaft (DFG) - EXC 2056 - project ID 390715994. C.S.M. acknowledges that the project that gave rise to these results received support via a fellowship from la Caixa Foundation (Grant No. 100010434) and from the European Union Horizon 2020 research and innovation program under the Marie Skłodowska Curie Grant Agreement No. 847648, with fellowship code No. LCF/BQ/PI20/11760026, and financial support from the Proyecto Sinérgico CAM 2020 Grant No. Y2020/TCS-6545 (NanoQuCo-CM).

APPENDIX A: LINDBLADIAN FOR TWO-PHOTON-ABSORPTION PROCESSES

In this Appendix we provide some details concerning the derivation of the Lindbladian for TPA given in Eq. (1) by drawing heavily on Refs. [59,63,65]. We are interested in two-photon-absorption processes in which the sample consists of an ensemble of independent two-level systems and transition between these levels is done by absorption from a single mode of the electromagnetic field. The number of these two-level systems is kept constant. The interaction Hamiltonian is given by

$$H_I = \sum_i (\xi \sigma_{2i}^\dagger \sigma_{1i} E^{+2}(\vec{r}_i) + \text{H.c.}), \tag{A1}$$

where ξ is the matrix element for TPA and $\sigma_{1i}^\dagger$ and $\sigma_{2i}^\dagger$ are the creation operators for the ith two-level system in two different states. The positive-frequency part of the electric field (in CGS units) is given by

$$E^+(\vec{r}_i) = -i\sqrt{2\pi\hbar\omega}u(\vec{r}_i)a, \tag{A2}$$

with $u(\vec{r}_i)$ the mode eigenfunctions. In general, based on the Liouville equation of motion, the total density operator of the matter-photon field satisfies the von Neumann equation

$$i\hbar\frac{\partial\rho_T(t)}{\partial t} = [\hat{H}_I, \rho_T(t)], \tag{A3}$$

where the operators are presented in interaction picture. At $t = 0$, the photon field and two-level systems of the sample are decoupled, indicating

$$\rho_T(0) = \rho(0) \bigotimes \prod_i \rho(0)_i, \tag{A4}$$

in which $\rho(0)_i$ is the thermal-equilibrium density operator for the ith two-level system. It should be noted that the density operator of the photon field at time t can be obtained by $\rho(t) = \text{Tr}_i \rho_T(t)$, in which Tr_i denotes the trace over two-level systems. Using the standard perturbation techniques based on Born-Markov approximations, we find the master equations

$$\begin{aligned}\frac{\partial\rho(t)}{\partial t} &= \frac{\kappa_1\gamma_{\text{TPA}}}{4}\{[a^2\rho(t), a^{\dagger 2}] + [a^2, \rho(t)a^{\dagger 2}]\} \\ &+ \frac{\kappa_2\gamma_{\text{TPA}}}{4}\{[a^{\dagger 2}\rho(t), a^2] + [a^{\dagger 2}, \rho(t)a^2]\},\end{aligned} \tag{A5}$$

where the first (second) line describes the absorption (emission) process, κ_1 (κ_2) is the thermal population of the two-level systems, and γ_{TPA} is given by [59,63]

$$\gamma_{\text{TPA}} = 2(2\pi)^2\omega^2|\zeta|^2 g(2\omega)\int d^3r\, N(\vec{r})|u(\vec{r})|^4, \tag{A6}$$

in which $g(2\omega)$ is the line-shape function and $N(\vec{r})$ is the density of atoms at the position $\vec{r}$ and integration takes place over volume of the medium. We assumed that the sample is at zero temperature; hence $\kappa_2 = 0$ and $\kappa_1 = 1$ and by redefinition of the creation and annihilation operators, Eq. (A5) would result in the Lindbladian given in (1).

APPENDIX B: DESCRIPTION OF SINGLE-PHOTON LOSSES VIA BEAM-SPLITTER TRANSFORMATION

Here we elaborate on why it is acceptable to model single-photon losses via an imbalanced beam-splitter transformation. For this presentation, we rely heavily on Chap. 5 of Ref. [69]. We show that there are two different but equivalent ways to describe the single-photon losses in our apparatus. One of these methods derives a Markovian master equation by tracing out the environmental degrees of freedom. In the other approach, we use the quantum Langevin equation of motion of the photon annihilation operator to find an input-output relation for the single-photon-loss processes.

We consider our propagating light field characterized by destruction operator a interacting with an environment (continuum of harmonic oscillators) characterized by destruction operator $b(\Delta)$, where Δ is the frequency of the environmental mode. The Hamiltonian for such a system and its environment in the interaction picture is given by [69]

$$\begin{aligned}H_I &= \hbar\int \Delta b^\dagger(\Delta)b(\Delta)d\Delta \\ &+ \hbar\int W(\Delta)[a^\dagger b(\Delta) + ab(\Delta)^\dagger]d\Delta.\end{aligned} \tag{B1}$$

We next transform it to the interaction picture with respect to the first term in Eq. (B1) (see Chap. 2 of [69] for more details), giving us the time-dependent Hamiltonian

$$V_I(t) = \hbar\int W(\Delta)[a^\dagger b(\Delta)e^{-i\Delta t} + ab(\Delta)^\dagger e^{i\Delta t}]d\Delta. \tag{B2}$$

It is straightforward to write the interaction Hamiltonian as

$$V_I(t) = i\hbar[a^\dagger F(t) - aF(t)^\dagger], \tag{B3}$$

in which we use the definition

$$F(t) = -i\int W(\Delta)b(\Delta)e^{-i\Delta t}d\Delta. \tag{B4}$$

The time evolution of the total density matrix describing the system and environment is given by

$$i\hbar\frac{\partial\rho_T(t)}{\partial t} = [V_I, \rho_T(t)], \tag{B5}$$

which by integrating it we get

$$\rho_T(t) = \rho_T(0) - \frac{i}{\hbar}\int [V_I(t'), \rho_T(t')]dt'. \tag{B6}$$

Considering that we are interested in the system (not the environment), we can trace out the effects of the environment (similar to Appendix A) and find

$$\frac{\partial\rho(t)}{\partial t} = -\frac{i}{\hbar}\mathrm{Tr}_e[V_I(t), \rho_T(t)] - \frac{1}{\hbar^2}\int_0^t \mathrm{Tr}_e[V_I(t'), [V_I(t'), \rho_T(t')]]dt', \tag{B7}$$

in which the first term is zero since it only contains a term proportional to $\langle F(t)\rangle$. Therefore, the only contributing term is the second term. By expanding this term and solving the integral accordingly (see Chap. 5 in Ref. [69] for more details), we will get

$$\frac{\partial\rho(t)}{\partial t} = \gamma_{\mathrm{SPA}}(2a\rho a^\dagger - a^\dagger a^\rho - \rho a^\dagger a), \tag{B8}$$

in which $\gamma_{\mathrm{SPA}} = \pi W(0)^2$ and this is the Lindbladian equation describing the single-photon-loss process in our optical setup.

Next we use the quantum Langevin equation to obtain an input-output relation. To this end, we conduct our study in the interaction picture, which means that $a \to a(t)$ and $b(\Delta) \to b(\Delta, t)$ in the interaction Hamiltonian in Eq. (B1). The equation of the motion for annihilation operator in Heisenberg picture gives us

$$\frac{\partial a(t)}{\partial t} = \frac{i}{\hbar}[H_I, a(t)] = -i\int W(\Delta)b(\Delta, t)d\Delta. \tag{B9}$$

It is a matter of straightforward calculation to find the solution of this differential equation as (see Chap. 5 in Ref. [69] for more details)

$$a(t) = e^{-\gamma_{\mathrm{SPA}}t}a(0) - iW(0) \times \int \frac{b(\Delta, 0)}{\gamma_{\mathrm{SPA}} - i\Delta}(e^{-i\Delta t} - e^{-\gamma_{\mathrm{SPA}}t})d\Delta, \tag{B10}$$

where, crucially, γ_{SPA} is identical to the loss rate in the above Lindblad equation (B8). If we take t to correspond to the time it takes for the light field to travel through the region where single-photon losses take place, we identify in Eq. (17) $a(t) = a'''$ and $a(0) = a''$. Furthermore, defining $e^{-\gamma_{\mathrm{SPA}}t} = \sqrt{\eta}$ and the second term in Eq. (B10) as $\sqrt{1-\eta}c$, where c can be shown to satisfy bosonic commutation relations, we find

$$a_{\mathrm{output}} = a''' = \sqrt{\eta}a'' + \sqrt{1-\eta}c, \tag{B11}$$

which is identical to beam-splitter transformation given in Eq. (17).

APPENDIX C: SINGLE-PHOTON LOSSES INSIDE THE TPA MEDIUM

Here we elaborate how single-photon losses taking place inside the TPA medium can be included in our analysis. In molecular TPA, these losses could stem from, e.g., photons scattering off the solution containing the TPA-active molecules, i.e., from the contribution of a second species of molecules in the target area. In an atomic setting, they might stem from a second atomic species which is admixed to the sample. In such a situation, the evolution equation is given by

$$\frac{d}{dt}\rho = (\gamma_{\mathrm{TPA}}\mathcal{L}_{\mathrm{TPA}} + \gamma_{\mathrm{SPA}}\mathcal{L}_{\mathrm{SPA}})\rho, \tag{C1}$$

where the first term is defined in Eq. (1) and the second term accounts for the single-photon losses and is given in Eq. (B8).

We first note that the two superoperators in Eq. (C1) do not commute, as it makes a difference whether photons are lost before or after interacting with the TPA sample. This complicates evaluating the change due to TPA losses. The formal solution of Eq. (C1) is given by

$$\rho(t) = \exp(\mathcal{L}_{\mathrm{TPA}}\varepsilon + \mathcal{L}_{\mathrm{SPA}}\varepsilon_s)\rho_0, \tag{C2}$$

where we define $\varepsilon_s = \gamma_{\mathrm{SPA}} \times t$ in addition to the notation introduced in the main text. In the main text we evaluated the change due to TPA losses perturbatively at $\varepsilon = 0$. This is well justified since these losses are typically small. However, in general, we cannot do the same for the single-photon losses, so we have to treat them to all orders in ε_s.

Using the Suzuki-Trotter formula, we next evaluate

$$\frac{\partial}{\partial\varepsilon}\exp(\mathcal{L}_{\mathrm{TPA}}\varepsilon + \mathcal{L}_{\mathrm{SPA}}\varepsilon_s) \tag{C3}$$

$$= \frac{\partial}{\partial\varepsilon}\left[\lim_{N\to\infty}\exp\left(\frac{\mathcal{L}_{\mathrm{SPA}}\varepsilon_s}{N}\right)\exp\left(\frac{\mathcal{L}_{\mathrm{TPA}}\varepsilon}{N}\right)\right]^N\Bigg|_{\varepsilon=0} \tag{C4}$$

$$= \lim_{N\to\infty}\frac{1}{N}\sum_{k=1}^{N}\exp\left(\frac{N-k}{N}\mathcal{L}_{\mathrm{SPA}}\varepsilon_s\right)\mathcal{L}_{\mathrm{TPA}}\exp\left(\frac{k}{N}\mathcal{L}_{\mathrm{SPA}}\varepsilon_s\right) \tag{C5}$$

$$= \int_0^1 dk\ \exp[(1-k)\mathcal{L}_{\mathrm{SPA}}\varepsilon_s]\mathcal{L}_{\mathrm{TPA}}\exp(k\mathcal{L}_{\mathrm{SPA}}\varepsilon_s). \tag{C6}$$

Thus, losses taking place during the photon propagation through the TPA medium can be included in the present analysis through a convolution of losses taking place before and losses taking place after the TPA event happened. Each of these events can be implemented with a beam-splitter transformation with transmission coefficients $\eta_{\mathrm{before}} = \exp(-2k\varepsilon_s)$ and $\eta_{\mathrm{after}} = \exp[-2(1-k)\varepsilon_s]$, followed by a simple integral over k. The total single-photon loss is then given by $\eta_{\mathrm{total}} = \eta_{\mathrm{before}}\eta_{\mathrm{after}} = \exp(-2\varepsilon_s)$.

We next consider how this affects intensity measurements with a squeezed vacuum state (19). A straightforward calculation yields

$$\frac{\partial}{\partial\varepsilon}\langle\hat{n}(k)\rangle_{\mathrm{SV}} = -\eta_{\mathrm{after}}\eta_{\mathrm{before}}^2 n_r(1+3n_r). \tag{C7}$$

Losses taking place before the TPA event contribute quadratically. The variance reads simply $\mathrm{Var}(\hat{n}) = \eta_{\mathrm{total}} n_r[1 + \eta_{\mathrm{total}}(1 + 2n_r)]$, i.e., here losses before and after the TPA event contribute linearly as before and the variance becomes independent of k. This shows that, as expected, losses before the TPA event cannot be compensated by a suitable measurement setup. Integrating over k, we obtain

$$\frac{\partial}{\partial\varepsilon}\langle\hat{n}\rangle_{\mathrm{SV}} = \int_0^1 dk \frac{\partial}{\partial\varepsilon}\langle\hat{n}(k)\rangle_{\mathrm{SV}} = -\eta_{\mathrm{total}} n_r(1 + 3n_r)\frac{\eta_{\mathrm{total}} - 1}{\ln(\eta_{\mathrm{total}})}. \tag{C8}$$

Here the first term with $\eta_{\mathrm{total}} = \eta_{\mathrm{before}}\eta_{\mathrm{after}}$ looks like single-photon losses acting on the state after the TPA event. By identifying $\eta = \eta_{\mathrm{total}}$, it reproduces the result of the main text. The losses before the TPA are accounted for by the extra term $(\eta_{\mathrm{total}} - 1)/\ln(\eta_{\mathrm{total}})$, which stems from the k integration of the second η_{before} in Eq. (C7).

Thus, overall, the sensitivity for photon-number measurements in the presence of single-photon losses inside the TPA medium evaluates to

$$\Delta\varepsilon_{\hat{n}}^{2\mathrm{SV}} \to \frac{2}{(3n_r)^2}\frac{\ln^2(\eta_{\mathrm{total}})}{(1 - \eta_{\mathrm{total}})^2}, \tag{C9}$$

where we find the second term stemming from these losses inside the TPA medium.

We also provide the calculation for intensity measurements with a coherent state, i.e., the result analogous to Eq. (24). We find

$$\Delta\varepsilon_{\hat{n}}^{2\mathrm{coh}} = \frac{1}{\eta_{\mathrm{total}} n_\alpha^3}\frac{\ln^2(\eta_{\mathrm{total}})}{(1 - \eta_{\mathrm{total}})^2}, \tag{C10}$$

where the first term is identical to Eq. (24) when we identify $\eta = \eta_{\mathrm{total}}$, but in addition we find the same term $\ln^2(\eta_{\mathrm{total}})/(1 - \eta_{\mathrm{total}})^2$ as in the squeezed vacuum case.

The exact same calculation can be repeated for quadrature measurements as well. We can calculate the sensitivity by replacing in Eqs. (40) and (42) the transmission probability η by η_{total} in the first line and by $\eta_{\mathrm{total}}\eta_b^2$ in the respective second lines. The variances are obtained by simply replacing η with η_{total}. Altogether, the sensitivity for quadrature measurements remains the same as in Eqs. (44) and (46), when we identify η in the above equations with η_{total} and add the additional factor that stems from the k integration, i.e.,

$$\Delta\varepsilon_{\hat{q}/\hat{p}}^2 \to \Delta\varepsilon_{\hat{q}/\hat{p}}^2 \frac{\ln^2(\eta_{\mathrm{total}})}{(1 - \eta_{\mathrm{total}})^2}. \tag{C11}$$

Hence, our results in the main text also hold for single-photon losses *inside* the TPA medium, provided the additional reduction factor $\ln^2(\eta_{\mathrm{total}})/(1 - \eta_{\mathrm{total}})^2$ is added, which accounts for losses taking place before the TPA event and which creates a reduction that appears independent of the initial quantum states of light which we considered in this paper.

A similar analysis for the classical Fisher information would be feasible in principle, but numerically very involved.

[1] D. N. Klyshko, Transverse photon bunching and two-photon processes in the field of parametrically scattered light, Sov. Phys. JETP **56**, 753 (1982).

[2] J. Gea-Banacloche, Two-Photon Absorption of Nonclassical Light, Phys. Rev. Lett. **62**, 1603 (1989).

[3] J. Javanainen and P. L. Gould, Linear intensity dependence of a two-photon transition rate, Phys. Rev. A **41**, 5088 (1990).

[4] N. P. Georgiades, E. S. Polzik, K. Edamatsu, H. J. Kimble, and A. S. Parkins, Nonclassical Excitation for Atoms in a Squeezed Vacuum, Phys. Rev. Lett. **75**, 3426 (1995).

[5] N. P. Georgiades, E. S. Polzik, and H. J. Kimble, Atoms as nonlinear mixers for detection of quantum correlations at ultrahigh frequencies, Phys. Rev. A **55**, R1605 (1997).

[6] B. Dayan, A. Pe'er, A. A. Friesem, and Y. Silberberg, Two Photon Absorption and Coherent Control with Broadband Down-Converted Light, Phys. Rev. Lett. **93**, 023005 (2004).

[7] B. Dayan, A. Pe'er, A. A. Friesem, and Y. Silberberg, Nonlinear Interactions with an Ultrahigh Flux of Broadband Entangled Photons, Phys. Rev. Lett. **94**, 043602 (2005).

[8] D.-I. Lee and T. Goodson, Entangled photon absorption in an organic porphyrin dendrimer, J. Phys. Chem. B **110**, 25582 (2006).

[9] A. R. Guzman, M. R. Harpham, O. Süzer, M. M. Haley, and T. G. Goodson, Spatial control of entangled two-photon absorption with organic chromophores, J. Am. Chem. Soc. **132**, 7840 (2010).

[10] L. Upton, M. Harpham, O. Suzer, M. Richter, S. Mukamel, and T. Goodson, Optically excited entangled states in organic molecules illuminate the dark, J. Phys. Chem. Lett. **4**, 2046 (2013).

[11] J. P. Villabona-Monsalve, O. Calderón-Losada, M. Nuñez Portela, and A. Valencia, Entangled two photon absorption cross section on the 808 nm region for the common dyes zinc tetraphenylporphyrin and rhodamine B, J. Phys. Chem. A **121**, 7869 (2017).

[12] J. P. Villabona-Monsalve, O. Varnavski, B. A. Palfey, and T. Goodson, Two-photon excitation of flavins and flavoproteins with classical and quantum light, J. Am. Chem. Soc. **140**, 14562 (2018).

[13] T. Li, F. Li, C. Altuzarra, A. Classen, and G. S. Agarwal, Squeezed light induced two-photon absorption fluorescence of fluorescein biomarkers, Appl. Phys. Lett. **116**, 254001 (2020).

[14] D. Tabakaev, M. Montagnese, G. Haack, L. Bonacina, J.-P. Wolf, H. Zbinden, and R. T. Thew, Energy-time-entangled two-photon molecular absorption, Phys. Rev. A **103**, 033701 (2021).

[15] R. K. Burdick, G. C. Schatz, and T. Goodson, Enhancing entangled two-photon absorption for picosecond quantum spectroscopy, J. Am. Chem. Soc. **143**, 16930 (2021).

[16] T. Landes, M. Allgaier, S. Merkouche, B. J. Smith, A. H. Marcus, and M. G. Raymer, Experimental feasibility of molecular two-photon absorption with isolated time-frequency-entangled photon pairs, Phys. Rev. Res. **3**, 033154 (2021).

[17] T. Landes, M. G. Raymer, M. Allgaier, S. Merkouche, B. J. Smith, and A. H. Marcus, Quantifying the enhancement of two-photon absorption due to spectral-temporal entanglement, Opt. Express **29**, 20022 (2021).

[18] M. G. Raymer, T. Landes, M. Allgaier, S. Merkouche, B. J. Smith, and A. H. Marcus, How large is the quantum enhancement of two-photon absorption by time-frequency entanglement of photon pairs? Optica **8**, 757 (2021).

[19] K. M. Parzuchowski, A. Mikhaylov, M. D. Mazurek, R. N. Wilson, D. J. Lum, T. Gerrits, C. H. Camp, M. J. Stevens, and R. Jimenez, Setting Bounds on Entangled Two-Photon Absorption Cross Sections in Common Fluorophores, Phys. Rev. Appl. **15**, 044012 (2021).

[20] K. E. Dorfman, F. Schlawin, and S. Mukamel, Nonlinear optical signals and spectroscopy with quantum light, Rev. Mod. Phys. **88**, 045008 (2016).

[21] F. Schlawin, Entangled photon spectroscopy, J. Phys. B **50**, 203001 (2017).

[22] F. Schlawin, K. E. Dorfman, and S. Mukamel, Entangled two-photon absorption spectroscopy, Acc. Chem. Res. **51**, 2207 (2018).

[23] M. Gilaberte Basset, F. Setzpfandt, F. Steinlechner, E. Beckert, T. Pertsch, and M. Graefe, Perspectives for applications of quantum imaging, Laser Photon. Rev. **13**, 1900097 (2019).

[24] S. Szoke, H. Liu, B. P. Hickam, M. He, and S. K. Cushing, Entangled light-matter interactions and spectroscopy, J. Mater. Chem. C **8**, 10732 (2020).

[25] S. Mukamel, M. Freyberger, W. Schleich, M. Bellini, A. Zavatta, G. Leuchs, C. Silberhorn, R. W. Boyd, L. L. Sánchez-Soto, A. Stefanov, M. Barbieri, A. Paterova, L. Krivitsky, S. Shwartz, K. Tamasaku, K. Dorfman, F. Schlawin, V. Sandoghdar, M. Raymer, A. Marcus *et al.*, Roadmap on quantum light spectroscopy, J. Phys. B **53**, 072002 (2020).

[26] Y.-Z. Ma and B. Doughty, Nonlinear optical microscopy with ultralow quantum light, J. Phys. Chem. A **125**, 8765 (2021).

[27] A. Eshun, O. Varnavski, J. P. Villabona-Monsalve, R. K. Burdick, and T. Goodson, Entangled photon spectroscopy, Acc. Chem. Res. **55**, 991 (2022).

[28] M. G. Raymer and T. Landes, Theory of two-photon absorption with broadband bright squeezed vacuum, Phys. Rev. A **106**, 013717 (2022).

[29] M. Bondani, A. Allevi, G. Zambra, M. G. A. Paris, and A. Andreoni, Sub-shot-noise photon-number correlation in a mesoscopic twin beam of light, Phys. Rev. A **76**, 013833 (2007).

[30] T. S. Iskhakov, V. C. Usenko, U. L. Andersen, R. Filip, M. V. Chekhova, and G. Leuchs, Heralded source of bright multimode mesoscopic sub-Poissonian light, Opt. Lett. **41**, 2149 (2016).

[31] L. Beltran, G. Frascella, A. M. Perez, R. Fickler, P. R. Sharapova, M. Manceau, O. V. Tikhonova, R. W. Boyd, G. Leuchs, and M. V. Chekhova, Orbital angular momentum modes of high-gain parametric down-conversion, J. Opt. **19**, 044005 (2017).

[32] M. V. Chekhova, S. Germanskiy, D. B. Horoshko, G. K. Kitaeva, M. I. Kolobov, G. Leuchs, C. R. Phillips, and P. A. Prudkovskii, Broadband bright twin beams and their upconversion, Opt. Lett. **43**, 375 (2018).

[33] P. R. Sharapova, G. Frascella, M. Riabinin, A. M. Pérez, O. V. Tikhonova, S. Lemieux, R. W. Boyd, G. Leuchs, and M. V. Chekhova, Properties of bright squeezed vacuum at increasing brightness, Phys. Rev. Res. **2**, 013371 (2020).

[34] J. Flórez, J. S. Lundeen, and M. V. Chekhova, Pump depletion in parametric down-conversion with low pump energies, Opt. Lett. **45**, 4264 (2020).

[35] K. Y. Spasibko, D. A. Kopylov, V. L. Krutyanskiy, T. V. Murzina, G. Leuchs, and M. V. Chekhova, Multiphoton Effects Enhanced due to Ultrafast Photon-Number Fluctuations, Phys. Rev. Lett. **119**, 223603 (2017).

[36] G. Brida, L. Caspani, A. Gatti, M. Genovese, A. Meda, and I. R. Berchera, Measurement of Sub-Shot-Noise Spatial Correlations without Background Subtraction, Phys. Rev. Lett. **102**, 213602 (2009).

[37] G. Brida, M. Genovese, and I. Ruo Berchera, Experimental realization of sub-shot-noise quantum imaging, Nat. Photon. **4**, 227 (2010).

[38] E. D. Lopaeva, I. Ruo Berchera, I. P. Degiovanni, S. Olivares, G. Brida, and M. Genovese, Experimental Realization of Quantum Illumination, Phys. Rev. Lett. **110**, 153603 (2013).

[39] R. B. de Andrade, H. Kerdoncuff, K. Berg-Sørensen, T. Gehring, M. Lassen, and U. L. Andersen, Quantum-enhanced continuous-wave stimulated Raman scattering spectroscopy, Optica **7**, 470 (2020).

[40] C. A. Casacio, L. S. Madsen, A. Terrasson, M. Waleed, K. Barnscheidt, B. Hage, M. A. Taylor, and W. P. Bowen, Quantum-enhanced nonlinear microscopy, Nature (London) **594**, 201 (2021).

[41] O. Varnavski and T. Goodson, Two-photon fluorescence microscopy at extremely low excitation intensity: The power of quantum correlations, J. Am. Chem. Soc. **142**, 12966 (2020).

[42] P.-A. Moreau, E. Toninelli, T. Gregory, and M. J. Padgett, Imaging with quantum states of light, Nat. Rev. Phys. **1**, 367 (2019).

[43] P. R. Tapster, S. F. Seward, and J. G. Rarity, Sub-shot-noise measurement of modulated absorption using parametric down-conversion, Phys. Rev. A **44**, 3266 (1991).

[44] E. S. Polzik, J. Carri, and H. J. Kimble, Spectroscopy with Squeezed Light, Phys. Rev. Lett. **68**, 3020 (1992).

[45] P.-A. Moreau, J. Sabines-Chesterking, R. Whittaker, S. K. Joshi, P. M. Birchall, A. McMillan, J. G. Rarity, and J. C. F. Matthews, Demonstrating an absolute quantum advantage in direct absorption measurement, Sci. Rep. **7**, 6256 (2017).

[46] F. Li, T. Li, M. O. Scully, and G. S. Agarwal, Quantum Advantage with Seeded Squeezed Light for Absorption Measurement, Phys. Rev. Appl. **15**, 044030 (2021).

[47] P. M. Birchall, E. J. Allen, T. M. Stace, J. L. O'Brien, J. C. F. Matthews, and H. Cable, Quantum Optical Metrology of Correlated Phase and Loss, Phys. Rev. Lett. **124**, 140501 (2020).

[48] G. S. Atkinson, E. J. Allen, G. Ferranti, A. R. McMillan, and J. C. F. Matthews, Quantum Enhanced Precision Estimation of Transmission with Bright Squeezed Light, Phys. Rev. Appl. **16**, 044031 (2021).

[49] P. Cutipa and M. V. Chekhova, Bright squeezed vacuum for two-photon spectroscopy: simultaneously high resolution in time and frequency, space and wavevector, Opt. Lett. **47**, 465 (2022).

[50] A. Svidzinsky, G. Agarwal, A. Classen, A. V. Sokolov, A. Zheltikov, M. S. Zubairy, and M. O. Scully, Enhancing stimulated Raman excitation and two-photon absorption using entangled states of light, Phys. Rev. Res. **3**, 043029 (2021).

[51] F. Schlawin, K. E. Dorfman, and S. Mukamel, Detection of photon statistics and multimode field correlations by Raman processes, J. Chem. Phys. **154**, 104116 (2021).

[52] Z. Zhang, T. Peng, X. Nie, G. S. Agarwal, and M. O. Scully, Entangled photons enabled time-frequency-resolved coherent

Raman spectroscopy and applications to electronic coherences at femtosecond scale, Light Sci. Appl. **11**, 274 (2022).
[53] O. Roslyak, C. A. Marx, and S. Mukamel, Nonlinear spectroscopy with entangled photons: Manipulating quantum pathways of matter, Phys. Rev. A **79**, 033832 (2009).
[54] Z. Yang, P. Saurabh, F. Schlawin, S. Mukamel, and K. E. Dorfman, Multidimensional four-wave-mixing spectroscopy with squeezed light, Appl. Phys. Lett. **116**, 244001 (2020).
[55] K. Dorfman, S. Liu, Y. Lou, T. Wei, J. Jing, F. Schlawin, and S. Mukamel, Multidimensional four-wave mixing signals detected by quantum squeezed light, Proc. Natl. Acad. Sci. USA **118**, e2105601118 (2021).
[56] Y. Michael, L. Bello, M. Rosenbluh, and A. Pe'er, Squeezing-enhanced raman spectroscopy, npj Quantum Inf. **5**, 81 (2019).
[57] Y. Michael, I. Jonas, L. Bello, M.-E. Meller, E. Cohen, M. Rosenbluh, and A. Pe'er, Augmenting the Sensing Performance of Entangled Photon Pairs through Asymmetry, Phys. Rev. Lett. **127**, 173603 (2021).
[58] C. Sánchez Muñoz, G. Frascella, and F. Schlawin, Quantum metrology of two-photon absorption, Phys. Rev. Res. **3**, 033250 (2021).
[59] G. Agarwal, Field-correlation effects in multiphoton absorption processes, Phys. Rev. A **1**, 1445 (1970).
[60] H. D. Simaan and R. Loudon, Quantum statistics of double-beam two-photon absorption, J. Phys. A: Math. Gen. **8**, 1140 (1975).
[61] H. D. Simaan and R. Loudon, Quantum statistics of single-beam two-photon absorption, J. Phys. A: Math. Gen. **8**, 539 (1975).
[62] H. D. Simaan and R. Loudon, Off-diagonal density matrix for single-beam two-photon absorbed light, J. Phys. A: Math. Gen. **11**, 435 (1978).
[63] M. S. Zubairy and J. J. Yeh, Photon statistics in multiphoton absorption and emission processes, Phys. Rev. A **21**, 1624 (1980).
[64] R. Loudon, Squeezing in resonance fluorescence, Opt. Commun. **49**, 24 (1984).
[65] L. Gilles and P. L. Knight, Two-photon absorption and nonclassical states of light, Phys. Rev. A **48**, 1582 (1993).
[66] Z. Y. Ou, Enhancement of the phase-measurement sensitivity beyond the standard quantum limit by a nonlinear interferometer, Phys. Rev. A **85**, 023815 (2012).
[67] D. Li, C. Yuan, Y. Yao, W. Jiang, M. Li, and W. Zhang, Effects of loss on the phase sensitivity with parity detection in an SU(1,1) interferometer, J. Opt. Soc. Am. B **35**, 1080 (2018).
[68] M. Manceau, G. Leuchs, F. Khalili, and M. Chekhova, Detection Loss Tolerant Supersensitive Phase Measurement with an SU(1,1) Interferometer, Phys. Rev. Lett. **119**, 223604 (2017).
[69] S. Barnett and P. Radmore, *Methods in Theoretical Quantum Optics* (Oxford University Press, Oxford, 2002).
[70] P. D. Drummond and Z. Ficek, *Quantum Squeezing* (Springer, Berlin, 2004).
[71] C. Gardiner and P. Zoller, *Quantum Noise* (Springer, Berlin, 2004).
[72] S. L. Braunstein and C. M. Caves, Statistical Distance and the Geometry of Quantum States, Phys. Rev. Lett. **72**, 3439 (1994).
[73] M. G. A. Paris, Quantum estimation for quantum technology, Int. J. Quantum Inf. **07**, 125 (2009).
[74] J. F. Haase, A. Smirne, S. F. Huelga, J. Kolodynski, and R. Demkowicz-Dobrzanski, Precision limits in quantum metrology with open quantum systems, Quantum Meas. Quantum Metrol. **5**, 13 (2016).
[75] R. Loudon, *The Quantum Theory of Light* (Oxford University Press, Oxford, 2002).
[76] T.-W. Lee, S. D. Huver, H. Lee, L. Kaplan, S. B. McCracken, C. Min, D. B. Uskov, C. F. Wildfeuer, G. Veronis, and J. P. Dowling, Optimization of quantum interferometric metrological sensors in the presence of photon loss, Phys. Rev. A **80**, 063803 (2009).
[77] M. Avenhaus, H. B. Coldenstrodt-Ronge, K. Laiho, W. Mauerer, I. A. Walmsley, and C. Silberhorn, Photon Number Statistics of Multimode Parametric Down-Conversion, Phys. Rev. Lett. **101**, 053601 (2008).